THESIS FOR THE DEGREE OF LICENTIATE OF ENGINEERING IN MACHINE AND VEHICLES SYSTEMS

Investigations of Flow Conditions in an Automotive Wind Tunnel

EMIL LJUNGSKOG

Department of Mechanics and Maritime Sciences

Division of Vehicle Engineering and Autonomous Systems

CHALMERS UNIVERSITY OF TECHNOLOGY

Göteborg, Sweden 2017

Investigations of Flow Conditions in an Automotive Wind Tunnel
EMIL LJUNGSKOG

Thesis for the degree of Licentiate of Engineering 2017:01
Department of Mechanics and Maritime Sciences
Division of Vehicle Engineering and Autonomous Systems
Chalmers University of Technology
SE-412 96 Göteborg
Sweden
Telephone: +46 (0)31-772 1000

Chalmers Reproservice
Göteborg, Sweden 2017

Investigations of Flow Conditions in an Automotive Wind Tunnel
Thesis for the degree of Licentiate of Engineering in Machine and Vehicles Systems
EMIL LJUNGSKOG
Department of Mechanics and Maritime Sciences
Division of Vehicle Engineering and Autonomous Systems
Chalmers University of Technology

Abstract

As vehicle manufacturers seek to shorten the development time of new models, wind tunnel testing of prototype vehicles needs to be partially replaced by virtual simulations. However, this requires thorough validation of the virtual methods, which is done by comparison to wind tunnel tests. Such comparisons are not straightforward, since a number of interference effects occur between the wind tunnel and the tested vehicle.

The objective of this thesis is to improve the understanding of two aspects of interference effects in the Volvo Cars slotted wall aerodynamic wind tunnel. The first aspect that is studied is the influence of six different boundary conditions, for the inlet and the moving ground system, on the longitudinal pressure gradient in numerical simulations of the tunnel. This is done with both steady-state and unsteady methods using a design of experiments approach. The results of the steady-state study show that the boundary layer scoop suction influences the pressure gradient throughout the whole test section, and that a smaller contribution to the pressure variations can be attributed to the two distributed suction systems. Changing the flow angularity on the inlet or varying the speed of the moving belts have shown no significant effect on the pressure distribution. Furthermore, the unsteady method provides better simulation accuracy than the steady-state procedure in the downstream region of the test section. This is attributed to a better representation of the shear layer in the open slots in the slotted walls.

The second aspect under consideration is the influence of the tangential blowing system that is part of the ground simulation in the wind tunnel. Using physical measurements, it is shown that the displacement thickness of the boundary layer is reduced by the blowing, and that non-uniformities in the thickness profile are present at interfaces between moving belts and stationary floor. Furthermore, it is shown that the force differences measured between different configurations of a vehicle can be significantly affected by the tangential blowing. The results indicate that vehicles with a larger base area are more sensitive to this phenomenon, and that configurations altering the underbody flow are more affected than those acting to change the flow in the base wake only. Furthermore, numerical simulations are used to trace the force differences between tangential blowing on and off to the rear of the vehicle. It is also demonstrated that the overall behaviour of the boundary layer downstream of the tangential blowers can be well represented in the simulations by using a simplified modeling approach for the blowing slots.

Keywords: Wind tunnel, Ground simulation, Tangential blowing, CFD simulations, Slotted walls

We came out of the cave, and we looked over the hill and we saw fire; and we crossed the ocean and we pioneered the west, and we took to the sky. The history of man is hung on a timeline of exploration and this is what's next.

Sam Seaborn

Acknowledgements

First of all I would like to thank my main supervisor, Associate Professor Simone Sebben, for all support and for the constructive comments on my writing when I have struggled. I would also like to thank my co-supervisors from Volvo Cars, Alexander Broniewicz and Dr. Christoffer Landström for the good discussions and all the help in the wind tunnel.

I would also like to thank Anders Lindroos and the others in the wind tunnel team at Volvo Cars for being helpful and patient all the times I want to run non-standard and somewhat contrived tests.

Furthermore, I want to thank FFI (Fordonsstrategisk Forskning och Innovation) and Volvo Cars for funding the project. A big thanks also to Professor Lennart Löfdahl, without whom this project would not have been possible.

Finally, I want to thank my colleagues at the division of Vehicle Engineering and Autonomous Systems for a fun and inspiring working environment, with a special thank you to my fellow Ph.D. students in the Road Vehicle Aerodynamics group for the excellent discussions on all kinds of topics.

Nomenclature

α	Flow pitch angle	$[^\circ]$
β	Flow yaw angle	$[^\circ]$
γ	Ratio of specific heats	$[-]$
δ	Boundary layer thickness	[m]
δ^*	Displacement thickness	[m]
Δt	Time step	[s]
C_D	Drag coefficient	$[-]$
C_L	Lift coefficient	$[-]$
C_{LF}	Front lift coefficient	$[-]$
C_{LR}	Rear lift coefficient	$[-]$
C_P	Pressure coefficient	$[-]$
P_s	Static pressure	$\left[\frac{\mathrm{N}}{\mathrm{m}^2}\right]$
P_t	Total pressure	$\left[\frac{\mathrm{N}}{\mathrm{m}^2}\right]$
q	Dynamic pressure	$\left[\frac{\mathrm{N}}{\mathrm{m}^2}\right]$
u	Local flow velocity	$\left[\frac{\mathrm{m}}{\mathrm{s}}\right]$
u_∞	Freestream velocity	$\left[\frac{\mathrm{m}}{\mathrm{s}}\right]$
y^+	Dimensionless wall distance	$[-]$

Abbreviations

BCD	Bounded Central Differencing
BLCS	Boundary Layer Control System
CFD	Computational Fluid Dynamics
GESS	Ground Effect Simulation System
IDDES	Improved Delayed Detached Eddy Simulation
ME	Lenth's Margin of Error
OAR	Open Area Ratio
PVT	Volvo Cars aerodynamic wind tunnel
RANS	Reynolds Averaged Navier-Stokes
SME	Lenth's Standard Margin of Error
WDU	Wheel Drive Unit
WLTP	Worldwide harmonized Light vehicles Test Procedure

Thesis

This thesis consists of an extended summary and the following appended papers:

Paper A E. Ljungskog et al. A Parametric Study on the Influence from Boundary Conditions on the Longitudinal Pressure Gradient in CFD simulations of an Automotive Wind Tunnel. *Journal of Mechanical Science and Technology* **Accepted for publication** (2017)

Paper B E. Ljungskog et al. On the Effects of Wind Tunnel Floor Tangential Blowing on the Aerodynamic Forces of Passenger Vehicles. *SAE International Journal of Passenger Cars - Mechanical Systems* **10(2)**.2017 (2017). DOI: 10.4271/2017-01-1518

Contents

Part I
Extended Summary

1 Introduction

Throughout the history of mankind, mobility has been one of the key enablers for exploration. Since the invention of the wheel, ground vehicles in different levels of technological refinement have been used to discover the world. In the society of today, mobility and transportation are perhaps more important to the masses than ever by enabling people to discover the world themselves. Especially the car has long been seen as a symbol for this personal freedom to go anywhere and explore, which has likely contributed to its vast popularity.

However, this popularity comes at a cost for the environment. In 2013, 17% of the global greenhouse emissions originated from ground transportation [3]. This has lead to a push from legislative authorities on the vehicle manufacturers to decrease the CO2 emissions of their vehicles. One way of reducing the emissions is to reduce the fuel consumption by lowering the aerodynamic drag that the vehicle has to overcome. Hence, a significant part of the development of a new vehicle is spent on optimizing its aerodynamic behaviour.

Apart from the legislative demands for reduced emissions, vehicle manufacturers today face increased demands from customers when it comes to as diverse attributes as design, safety and fuel consumption. This has lead to a situation where a vehicle can be perceived as outdated just a few years after having been released to the market. In order to bring new technology to the market as soon as possible, the time to develop a new vehicle needs to be reduced. As the manufactures strive to achieve such lead time reductions, new ways of working have to be employed to meet the often very ambitious time reduction goals. One such way of cutting down on both time and cost is to replace physical testing on prototype vehicles with virtual simulations. In the case of external aerodynamics, this means substituting wind tunnel testing with Computational Fluid Dynamics (CFD) simulations. However, thorough validation of the virtual methods has to be performed before they can fully replace physical testing.

The most straightforward way of validating a CFD simulation of the aerodynamic performance of a vehicle is to compare it to measurements from a wind tunnel. However, there are many possible error sources that complicate such a comparison. Except from potential shortcomings of the numerical method itself, there are also issues arising regarding the geometric representation of the test object. Furthermore, CFD simulations are typically performed by placing the vehicle inside a very large box-like "virtual wind tunnel", which shares little resemblance with the physical wind tunnel. Hence, no interference effects between the wind tunnel and the test object are taken into account, meaning that a proper validation of the computational method itself cannot be performed unless these interference effects are fully understood or the wind tunnel geometry is included in the simulations. An increased knowledge of the interference effects also allows for a better understanding of how the aerodynamic effects from different configurations evaluated in the wind tunnel compares to real world conditions.

The need to understand the wind tunnel interference is further accentuated by recent changes in the regulations for the fuel consumption certification of new vehicles. This new

set of rules, known as the Worldwide harmonized Light vehicles Test Procedure (WLTP) [4], mandates that not only the fuel consumption for the base variant of a vehicle is measured and reported, but that the effect of optional extras are also taken into account. If all combinations of extras that might influence the aerodynamics of the vehicle were to be tested in accordance to the old regulations, hundreds of time consuming and expensive coast-down tests would need to be performed for each new model. However, WLTP allows for the use of wind tunnel testing instead of coast-down tests if the tunnel fulfils certain criteria, which increases the need for a detailed understanding of how the wind tunnel influences the aerodynamic forces measured on the vehicle.

Furthermore, WLTP states that some wind tunnel tests can be substituted by CFD simulations if a set of requirements and restrictions are fulfilled, of which validation to wind tunnel data is one. Apart from requiring agreement between forces, the validation also demands that the simulations show similar flow patterns, velocities, and pressures, when compared to the wind tunnel. It is likely that inclusion of the wind tunnel into the simulation procedure is necessary in order to fulfill such requirements, further emphasising the need to understand the interference effects.

1.1 Objective

This work is part of a larger project, aiming at increasing the understanding of the properties of slotted wall wind tunnels in automotive aerodynamics. The project also aims at improving simulation accuracy by providing validation between CFD and wind tunnel measurements, as well as investigating the possibilities to base the requirements used during the vehicle development on virtual methods.

The work described in this thesis is geared toward the first goal of the project, and seeks to improve the understanding of two aspect of the tunnel under consideration; the longitudinal pressure distribution, and the effect from the tangential blowing subsystem of the moving ground system. This is done using both experimental and numerical methods.

1.2 Outline

The first part of the thesis concerns with some theory and background on automotive wind tunnels in general, and the slotted wall wind tunnel of main interest in this work in particular. This is followed by descriptions of the experimental and numerical methods used in the investigations of the longitudinal pressure gradient and the tangential blowing effects.

Succeeding the description of the methodology, the results of the investigations are presented and discussed, beginning with numerical investigations of the longitudinal pressure distribution using both steady-state and unsteady methods. After this, the results of the tangential blowing investigations are given.

The thesis ends with some conclusions and an outlook on further work, followed by the appended papers.

2 Automotive wind tunnels

In this chapter, a brief introduction to the field of automotive wind tunnels is given, starting with a discussion of boundary interference and the idea of building interference free wind tunnels. This is followed by a an overview of how the ground is simulated in wind tunnels and a glance on the literature on numerical simulations of wind tunnels. The chapter ends with a description of the wind tunnel under consideration in this work.

2.1 Boundary interference

The condition an automotive wind tunnel tries to simulate is the car driving on a flat plane in still air, meaning that the flow is only constrained by the flat plane, i.e. the ground. Since the flow in a wind tunnel test section is constrained by the test section boundaries, the flow conditions will not be the same as for the idealized case the tunnel is set to simulate. The effect from such constraints is called boundary interference, and can be divided into separate effects that are commonly assumed to be additive. Two of the most important boundary interference effects for automotive tunnels are the so called solid blockage and horizontal buoyancy, briefly discussed below for open jet and closed wall test sections. For a more in-depth discussion, see for example Cooper [5], Barlow et al. [6], or Pankhurst and Holder [7].

Solid blockage In a closed wall test section, the introduction of a blockage will cause an increase of the streamwise velocity in order for continuity to be fulfilled. This is because the walls do not allow for the streamlines to expand as they would in free air, as shown in Figure 2.1. This would lead to a higher velocity around the test object, and thus a higher measured drag.

For an open jet test section, the boundary condition of the jet is that of pressure equal to the plenum pressure, which is higher than the static pressure in the stream. This causes the streamlines to expand more than in free air, causing a decrease of the streamwise velocity in the vicinity of the test object and thus a lower measured drag.

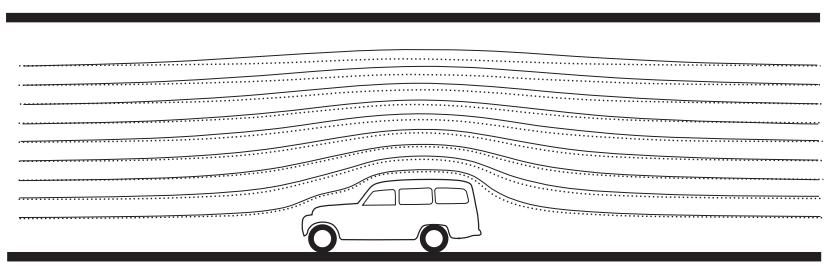

Figure 2.1: *Streamlines for open road (solid) and closed test section (dotted).*

Horizontal buoyancy Due to boundary layer buildup on the walls along the length of a closed wall test section, the inviscid core of the flow must accelerate slightly for the stream to fulfill continuity, leading to a decrease in pressure according to Bernoulli's principle. This axial pressure gradient will act as a buoyancy in the streamwise direction and will increase the measured drag.

In the open jet case, the axial pressure gradient is not mainly driven by the boundary layer buildup, but rather by the interaction with the nozzle and the collector. Normally, the pressure drops after the nozzle and rises before entering the collector [5]. This interaction can be avoided by placing the test object at a sufficient distance from both the nozzle and the collector. However, this is usually not possible since the usable length of an open test section is limited by the shear layer instability of the jet, meaning that the test object is typically located in a region influenced by either the nozzle or the collector.

2.2 Self-correcting wind tunnels

Considering the boundary interference effects described above, it can be noted that the sign of each effect can vary between the two different test section types, and for the horizontal buoyancy in an open jet even within the same test section. Therefore, it might be possible to build wind tunnels that are "self-correcting", for which all boundary interference effects cancel each other out. Two such approaches will be briefly discussed here; slotted walls and self-correcting open jet.

2.2.1 Slotted walls

Slotted walls are not commonly seen in automotive wind tunnels today. The concept originates from the aerospace industry, where large slotted wall wind tunnels have been used since 1949 [8]. A slotted wall test section have walls that are not solid, but has longitudinal openings into a plenum. The idea of the slotted walls is to decrease the strong boundary interference experienced in solid wall tunnels by allowing for the jet to expand through the slots when a blockage is introduced into the test section. This approach preserves the long usable length of a closed wall test section that would be limited by strong shear layer instabilities in an open jet.

In the early days of design of automotive slotted wall tunnels, there was a belief that the slotted wall design would allow for almost interference free testing [8–11], meaning that self-correcting wind tunnels would be feasible. However, Eng and Walker [12] showed that correction is necessary and proposed a method based on closed test section corrections.

2.2.2 Self-correcting open jet

In 1996, Mercker and Wiedemann [13] noted that interference correction for open jet tunnels could not be fully described by the previously known correction methods, and

introduced a new method. This approach lay the foundation for the theory of self-correcting open jet wind tunnels, as described by Wickern [14]. The core of his approach is to balance the solid blockage contributions from the nozzle and the over expansion of the jet by placing the test object closer or further from the nozzle, together with careful design of the collector. The approach of balancing the blockage contributions has some similarities to the slotted wall principle as Wickern notes, in that the behaviour of an open jet wind tunnel approaches that of a closed wall test section as the test object is placed closer to the nozzle.

2.3 Ground simulation

As noted above, the condition an automotive wind tunnel is supposed to simulate is the car driving on an open road in still air. However, in the wind tunnel the car is stationary and the air moves, meaning that the ground should move with the air in order to simulate the correct relative motion between the car and the road. The importance of providing the effect of this motion has been well described in the literature, for example by Wiedemann [15, 16]. One study of the effects of proper ground simulation that stands out is the one by Larsson et al. [17], who compared tests for a production car in a wind tunnel without a moving ground to experiments of the same car in a water filled towing tank that allowed for a correct relative motion between the car and the ground at a representative Reynolds number. They showed that while drag was similar between the two test methods, likely due to the fact that the drag decrease from the floor boundary layer in the wind tunnel was countered by a drag increase caused by the stationary wheels, the front lift could be as much as 50% higher in the tunnel. Furthermore, they showed that force differences due to changes of the upperbody of the car were well predicted by the wind tunnel, but that it failed at predicting differences caused by changes on the underbody.

Achieving a fully correct ground simulation is in principle possible by using a conveyor belt upon which the car is positioned. Unfortunately, this is impractical for full scale testing, since the car would need to be held in place by some external structure, which complicates force measurements significantly. This has lead to a number of techniques being developed to simulate the interaction between the car and the ground. The three most common techniques, namely moving belts, distributed suction, and tangential blowing, will be discussed here. It shall be noted that of the three, only the moving belts provide the correct kinematic boundary condition for the ground, while the two others aim at generating the correct ground interaction by means of boundary layer thickness reduction. However, in most modern wind tunnels all three methods are used in conjunction in order to exploit their strengths while mitigating their weaknesses.

2.3.1 Moving belts

The possibility of using a moving belt for ground simulation was introduced already by Gustave Eiffel [18], and realized by Klemin [19] in 1934. Given that the oncoming boundary

layer is completely removed upstream of the belt, the velocity profile at the model location is the same as on the road. However, the single belt approach is problematic, especially for full scale testing. Consequently, moving belts were not widely used until the last two decades, when many new wind tunnels were built, and existing tunnels upgraded with a moving ground system [20–27]. Typical for most of these tunnels is that they employ some variant of a so called five belt system, which consists of a long centre belt running in between the wheels under the car, and four separate wheel drive units that provide the wheel rotation. The car is typically held in place by four struts attached to the jacking points and connected to the underfloor balance. Some facilities even provide two different belt configurations; a five belt system for passenger vehicle testing and a single- [26] or three belt system [27] for race car testing.

Some of the possible belt configurations that can be used were investigated numerically by Hennig et al. [28]. They found that especially for racing cars with low ground clearance, the improved ground simulation provided by a single- or three belt system is necessary in order to measure lift accurately. Furthermore, they concluded that the improved aerodynamic simulation capabilities have to be weighed against the increased technical complexity of the few-belt systems compared to the five belt variant. This increase in complexity mainly stems from the fact that lift measurements have to be taken through the belt for the single- and three belt configurations, since a connection of the whole belts to the balance would lead to large parasitic forces.

2.3.2 Distributed suction

A possible approach to prohibit boundary layer growth on a surface is to use distributed suction. For an automotive wind tunnel, this is usually done by having a porous plate as the ground and applying suction through the plate, thus removing the fluid close to the ground including the boundary layer.

Despite its conceptual simplicity, distributed suction is associated with some difficulties. As noted by Hucho [18], determination of the correct suction rate is problematic. The suction rate is usually determined for an empty test section, for which it is adjusted to achieve a set displacement thickness at a given location. However, when a test object is introduced into the test section, the flow field changes substantially near the object, thus invalidating the conditions for which the suction rate was calibrated. Furthermore, the test object imposes a pressure distribution on the suction zone, which might change the distribution of the mass flow through the plate.

Apart from the calibration difficulties, Mercker and Wiedemann [29] showed that since it removes mass and momentum from the flow, distributed suction is unable to provide correct boundary conditions underneath a car. They also showed that it can cause significant flow angularity if suction is applied excessively. Wickern et al. [30] further showed that such excessive suction can have a large impact on the longitudinal pressure gradient and by that changing the measured drag. Due to these concerns, a typical usage of distributed suction is to remove the incoming boundary layer upstream of a moving belt system.

2.3.3 Tangential blowing

Another possibility to reduce the influence from the floor boundary layer is to fill in its momentum deficit by injecting a high speed jet parallel to the ground, which is the basic principle of tangential blowing.

One major shortcoming of tangential blowing is that the desired displacement thickness can only be obtained for one specific streamwise location. However, Mercker and Knape [31] showed that good agreement to moving ground measurements could be attained for drag by choosing this location as the location of the front wheels, even though this lead to an overprediction of lift.

Mercker and Wiedemann [29] concluded that tangential blowing has some advantages over distributed suction, despite its shortcomings. For example, the imposed flow angularity is significantly smaller than for suction, and the adverse effect of momentum removal seen from suction is avoided.

In modern installations, tangential blowing is often used in conjunction with moving belts and distributed suction. A typical use is to fill in the boundary layer created on the strip of stationary ground often found downstream of a distributed suction zone and upstream of a moving belt. Another use case is to mount the blowers just downstream of a belt in order to extend the apparent length of the belt.

2.4 Numerical simulation of wind tunnels

As discussed, the improved requirements on simulation accuracy has increased the need for inclusion of wind tunnel effects in numerical simulations during recent years. This has lead to a number of papers being published on the subject. The usual approach taken for simulation of automotive wind tunnels can be divided into two groups; using the standard box-type CFD simulation domain with inclusion of the ground simulation system from the physical wind tunnel, or inclusion of the full geometry of the contraction, test section and diffuser.

A case for not including the return circuit of the wind tunnel was made by Nayani et al. [32], who simulated the full geometry of a closed wall aeronautic wind tunnel, including fan and corner guide vanes. They concluded that the inclusion of the return leg was not straigthforward and required additional work; especially the modelling of the fan and the anti-turbulence nets proved to be problematic.

Many of the simulations of automotive wind tunnels described in the literature has been performed on open jet tunnels [33–37], with some exceptions for closed wall tunnels mainly used for testing of commercial vehicles [38, 39]. A general conclusion is that the simulation accuracy when compared to physical tests tends to increase when the wind tunnel geometry is taken into account. For example, Fischer et al. [34] simulated a detailed scale model of a notchback in two different configurations of an open jet wind tunnel, and compared the forces to both blockage free CFD simulations and measurements in the physical tunnel.

They found that for the one wind tunnel configuration with the larger interference effects, the accuracy of the CFD simulations improved when the wind tunnel geometry was included in the simulations, compared to the blockage free simulations. Furthermore, they noted that some of the differences seen between the physical force measurements and the simulations with included wind tunnel geometry corresponded to a difference between the measured and simulated longitudinal pressure distribution in the empty test section, and concluded that the pressure variations are important to capture in the simulations.

Some studies have also been performed for a slotted wall configuration [40–42]. The study of Perzon [40] was one of the first published on CFD simulations of wind tunnel interference in automotive aerodynamics. He concluded that the flow field of the simplified vehicle considered changes inside of the wind tunnel as compared to blockage free simulations. However, the simulation method used then does not meet modern standards in terms of for example mesh resolution, thus making conclusions uncertain. The more recent investigations of the same wind tunnel by Olander [41] and Wall [42] showed some discrepancies between the simulated and measured flow field in the empty test section, and hypothesised that the origin of these differences might have been caused by anomalies upstream of the simulated region, or by uncertainties in the modeling of the moving ground system.

2.5 Volvo Cars aerodynamic wind tunnel

The wind tunnel under consideration in this thesis is the Volvo Cars full scale aerodynamic wind tunnel (PVT). An overview of PVT can be seen in Figure 2.2. The tunnel is located in Gothenburg, Sweden, and is of closed return (Göttingen) type with a slotted wall test section. The tunnel is equipped with systems for control of both temperature and humidity, making it capable of both aerodynamic and thermodynamic testing. When running thermodynamic tests, the test object is mounted on a dynamometer, which is located downstream of the turntable and force balance.

When the tunnel was built and commissioned in the mid 1980s, it was not equipped with a moving ground system. In 2006, it was upgraded with a 5 MW fan, allowing wind speeds of up to 250 km/h, and with a five belt moving ground system. A description of the upgrade was given by Sternéus et al. [23].

An overview of the technical specifications of the wind tunnel is provided in Table 2.1. Descriptions of the moving ground system, the test section flow quality, and the repeatability of the force measurements are given in the following sections.

2.5.1 Moving ground system

The five belt moving ground system in PVT is illustrated in Figure 2.3. Beginning at the nozzle outlet, the boundary layer control system starts with a basic suction scoop, driven by a separate 250 kW fan and capable of removing up to 30 m^3/s of air through its 75 mm

Table 2.1: Summary of the technical specifications of the Volvo Cars aerodynamic wind tunnel. The flow quality data is taken from the commissioning report [43].

Overall layout	
Type	Closed return (Göttingen)
Contraction ratio	6:1
Fan	5 MW with 9 blades, 8 m diameter
Test section	
Type	Slotted Walls
Open area ratio	30%
Dimensions	$6.6 \times 4.1 \times 15.8\,\mathrm{m}^3$ $(W \times H \times L)$
Cross-sectional area	$27.06\,\mathrm{m}^2$
Flow	
Maximum wind speed	250 km/h
Wind speed determination	Nozzle method, pressure drop between settling chamber and nozzle outlet
Dynamic pressure uniformity at turntable centre	$\sigma = 0.3\,\%$
Flow angle uniformity at turntable centre	$\sigma_\alpha = 0.29\,^\circ$ (Pitch)
	$\sigma_\beta = 0.18\,^\circ$ (Yaw)
Turbulence level at turntable centre	0.1%
Moving ground system	
Type	Five belts with boundary layer scoop, distributed suction and aft-belt tangential blowing
Boundary layer thickness at turntable centre	$\delta^* = 0.35\,\mathrm{mm}$
Velocity range	$7 - 260\,\mathrm{km/h}$
Turntable and balance	
Turntable diameter	6.6 m
Yaw angle range	$\pm 30^\circ$
Angle resolution	$\pm 0.05^\circ$
Balance	Pfister six component underfloor balance
Thermodynamics	
Temperature range	$20 - 60\,^\circ\mathrm{C}$
Relative humidity	$10 - 90\,\%$
Solar simulation	$816 - 1200\,\mathrm{W/m}^2$ full spectrum
Dynamometer	Located downstream of the turntable, 2WD, absorbing up to 225 kW

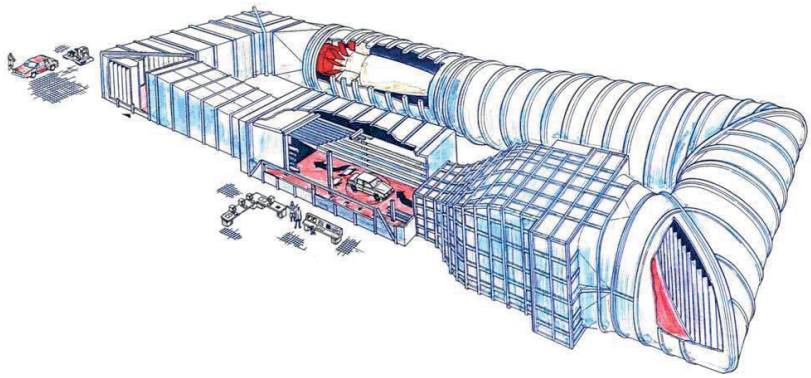

Figure 2.2: *Overview of the Volvo Cars aerodynamic wind tunnel (PVT).*

tall and 6030 mm wide opening. Its role is to take out the boundary layer buildup from the floor of the nozzle. The air removed by the scoop is reinjected above the slotted roof.

The floor area between the scoop and the turntable consists of a perforated floor, with an open area ratio of 8.9%, that constitutes the first distributed suction system able to remove up to 7.7 m^3/s. The second distributed suction system is very similar to the first, but with an open area ratio of 4.5% and a removal capacity of 2.05 m^3/s, and is mounted on the upstream part of the turntable. Most of the air removed by the distributed suction systems is injected back into the wind tunnel outside of the slotted walls.

A fraction of the air removed by the second distributed suction is reinjected through the tangential blowing system. This system consists of five separate blowers; one mounted downstream of each moving belt. The more common installation with tangential blowing upstream of the belts was rejected during the upgrade of the wind tunnel as it was deemed to be located too close to the front wing when testing Formula 1 cars [23]. Each WDU blower consists of a 0.6 mm tall and 600 mm wide slot, from which the air is exiting after passing through a settling chamber under the floor. The centre belt blower is similarly constructed, but with a 1 mm tall and 1 m wide blowing slot. All five blowers are pressurised by the same compressor, and can be individually adjusted either by a valve mounted before each settling chamber or by changing the slot height.

As previously mentioned, the rolling road itself consists of five separate belts. Each belt can be controlled individually, and does not have to follow the wind speed. The 0.8 mm thick steel centre belt is 1 m wide and 5.3 m long, and is suspended on two 590 mm rollers, of which the rear one is continually moved to adjust the tracking of the belt. In between the rollers, the belt is floating on an air lubrication system, consisting of alternating suction and blowing regions through porous graphite. This ensures that the belt does not overheat due to friction.

The floor on the turntable can be reconfigured and the four wheel drive units moved to account for different wheel bases and track widths within the ranges given in Table 2.2.

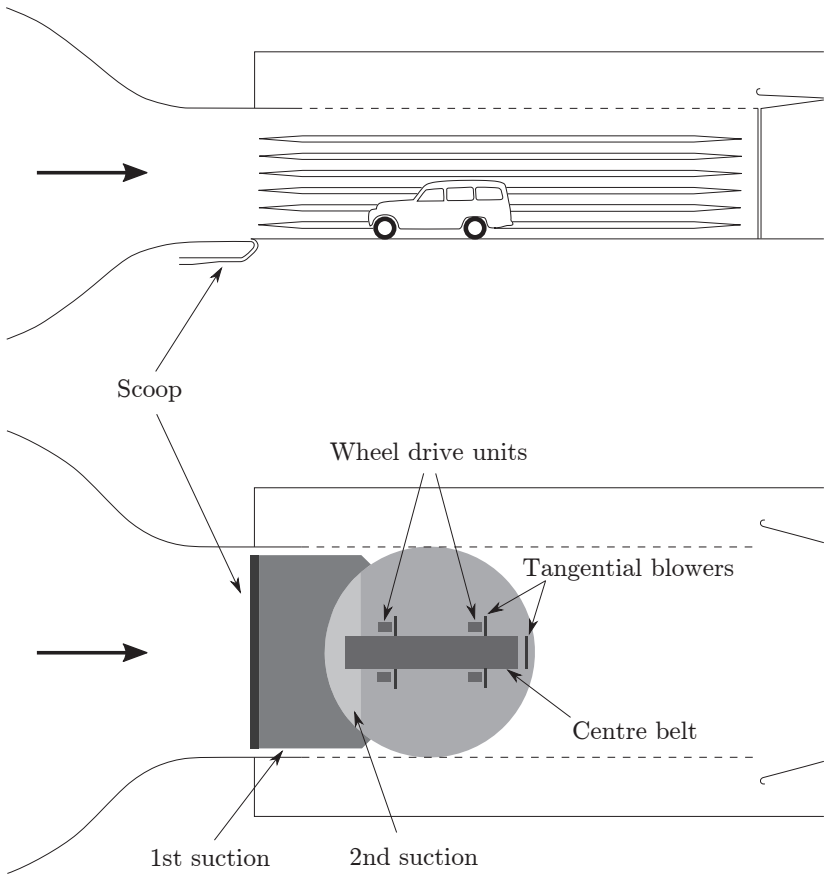

Figure 2.3: *Layout of the boundary layer control system in PVT.*

Table 2.2: Permissible wheel base and track width ranges in PVT.

Property	Min [mm]	Max [mm]
Track width	1380	1657
Wheel base	2032	3200

The WDU belts can be changed between three different widths, 280, 360, or 410 mm, in order to handle different tyre widths. In contrast to the centre belt, the wheel drive units are connected to the underfloor balance. Furthermore, load cells between each WDU and the balance frame allows for measurement of the tractive force needed to rotate each wheel to within ± 2 N. The same air lubrication method used for the centre belt is also used for the WDU belts.

While mounted on the turntable, the tested vehicle is held in place by four struts connected to the balance and the vehicle jacking points. These struts can be positioned independently of the wheel drive units to allow for different vehicle types to be tested. The vehicle ride height can be adjusted within the ± 50 mm stroke of the struts during a test, and the whole vehicle can be raised 400 mm between tests to enable configuration changes to the underbody. A second type of struts that does not constrain the vehicle movement in the vertical direction are also available. Using these "floating" struts allows for investigation of for example lift induced attitude changes.

Boundary layer thickness

The effect of the moving ground system can be seen in Figure 2.4, showing the boundary layer profiles at the turntable centre ($x = 0$, $y = 0$). Data is shown for three different operating modes for the moving ground system. In the aerodynamic mode, all systems described above are active, while in the GESS off (Ground Effect Simulation System off) mode, only the basic suction scoop and the two distributed suction systems are active. For the scoop only mode, all systems except for the scoop are turned off.

For the aerodynamic mode, a small velocity deficit can be seen. This is caused by an unavoidable step from the plate upstream of the belt down to the belt [23]. The deficit leads to a relatively thick boundary layer thickness of $\delta = 16$ mm, as shown in Table 2.3. However, since the deficit is rather small, the displacement thickness is only $\delta^* = 0.35$ mm.

As expected, the boundary layer is considerably thicker for the GESS off and scoop only modes. For the scoop only mode, the commissioning [43] showed that the boundary layer grows to a thickness of $\delta \approx 20$ mm over the distributed suction zones when they are deactivated, which causes the difference seen at the turntable centre in Table 2.3.

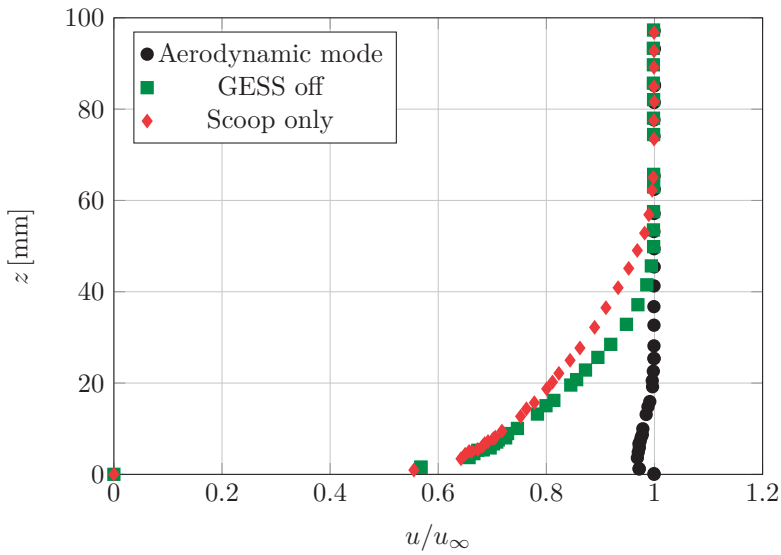

Figure 2.4: *Boundary layer profiles measured at the turntable centre at a freestream velocity of* $u_\infty = 200\,\mathrm{km/h}$. *Data from Sternéus et al. [23].*

Table 2.3: Boundary layer and displacement thickness at the turntable center for the different operating conditions in PVT. Data from Sternéus et al. [23].

Operating condition	δ [mm]	δ^* [mm]
Aerodynamic mode	16	0.35
GESS off	45	7.5
Scoop only	63	10.1

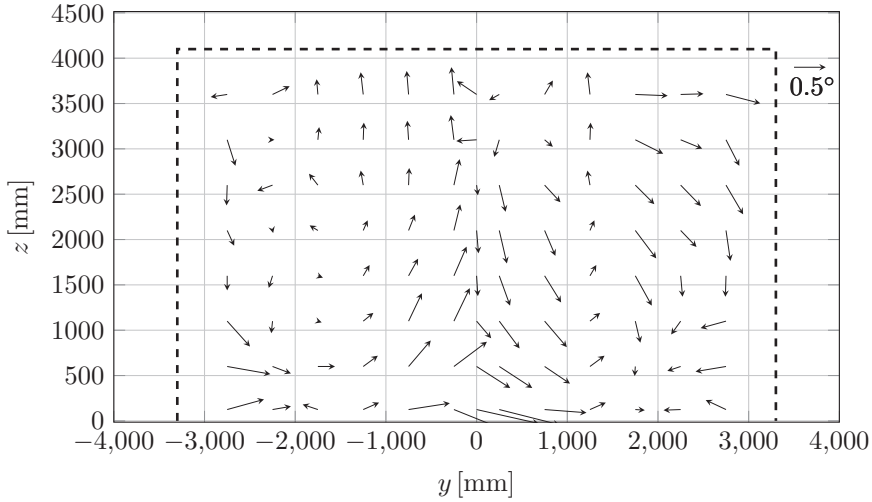

Figure 2.5: *Flow angles over a cross plane at the turntable centre for the aerodynamic mode of operation. Data from the commissioning report [43].*

2.5.2 Flow conditioning and quality

In order to provide good flow quality in the test section, a number of techniques are employed. Each corner has guide vanes to help realigning the flow, which both reduces power consumption and improves flow stability. In the settling chamber upstream of the contraction and nozzle, a total of four anti-turbulence screens are mounted, together with the heat exchanger and a honeycomb structure. Since the heat exchanger is a large loss device, it helps to make the flow more uniform before it enters the honeycomb for alignment. Downstream of these two devices, three of the screens act as smaller loss devices to further improve the spatial uniformity of the flow, as well as breaking down larger turbulent structures. The remaining small turbulent structures decay when the flow is accelerated through the 6:1 contraction.

These flow conditioning measures results in a low turbulence flow in the test section, as low as 0.1% on average over a cross plane located at the turntable centre. Furthermore, the dynamic pressure standard deviation over the same plane is $\sigma = 0.4\%$.

The flow angularity on the aforementioned plane is visualised in Figure 2.5 and summarized in Table 2.4. It can be seen that two vortical structures seems to be present in the flow, which has been present since the original commissioning in 1986 and has not been proven to be significant [23]. It has been hypothesised that this swirl originates from leakage around the heat exchanger in the settling chamber, but this has yet to be investigated.

Table 2.4: Statistics for flow angularity measured on a cross plane at the turntable centre for the aerodynamic mode of operation. Data from the commissioning report [43].

	Pitch angle [°]	Yaw angle [°]
Mean	-0.04	-0.13
Standard deviation (σ)	0.29	0.18
Maximum	0.52	0.32
Minimum	-0.52	-0.53

2.5.3 Force coefficient repeatability

As is the case for all physical measurements, the wind tunnel force measurements are associated with some degree of variability. The variability level in PVT is characterised by the repeatability of the measured force coefficients. Such a characterisation can be done in two ways; within a test and between two tests. For the former, the car stays mounted in the test section for all measurements, while for the latter the car is removed from the test section and reinstalled. For the measurements performed as a part of this thesis, all measurements were performed without removing the car, why the within test repeatability, shown in Table 2.5, is the more relevant of the two.

Table 2.5: Force coefficient repeatability within a test.

Force	Coefficient	Repeatability
Drag	C_D	± 0.001
Front lift	C_{LF}	± 0.001
Rear lift	C_{LR}	± 0.005

2.5.4 Coordinate system

The coordinate system in PVT is a right hand oriented system with its origin at the turntable centre. Positive z is directed upwards with $z = 0$ at the floor, and positive x is aligned with the flow. All coordinates throughout the remainder of this thesis are given in this coordinate system.

3 Methodology

In this chapter, the methodology used in the investigations is presented. The discussion begins with a description of the experimental approaches, which is followed by the methods used for the numerical studies.

3.1 Experimental studies

The experimental studies that have been part of the present work can be divided into two separate investigations; measurement of the longitudinal static pressure distribution in the test section, and exploration of the impact from the tangential blowing system on the boundary layer and on the forces measured for two different vehicle types in the wind tunnel.

3.1.1 Longitudinal static pressure distribution

Measurements of the static pressure gradient were performed using a Prandtl tube mounted on a custom built wing-shaped rig, shown in Figure 3.1.

The differential pressure between the total- and static pressure ports, denoted $P_{Prandtl}$, was measured using the wind tunnel differential pressure transducer. The pressure coefficient was then computed as

$$C_p = \frac{-P_{Prandtl} + k_q \Delta P_{nozzle} + k_p \Delta P_{nozzle}}{k_q \Delta P_{nozzle}} - \frac{k_p}{k_q}, \tag{3.1}$$

where ΔP_{nozzle} is the pressure drop over the nozzle used to calculate the freestream wind speed, and k_p and k_q are two calibration coefficients derived during the commissioning of the wind tunnel.

3.1.2 Tangential blowing system

The investigation of the influence of the tangential blowing system was divided into two parts. First, the uniformity of boundary layer thickness downstream of the tangential blowers was measured in the empty test section. This was then followed by investigations on the sensitivity to tangential blowing of the measured forces on different vehicle types and configurations.

Boundary layer thickness

The uniformity of the boundary layer thickness was measured using a rake of 22 total pressure probes mounted on the wind tunnel traversing gear, as shown in Figure 3.2. The

rake was swept across the width of each blower, at a downstream distance of 800 mm from the slot. This position was chosen to correspond with the position for which the tangential blowers were calibrated during commissioning [43].

As mentioned in section 2.3, there is typically a velocity overshoot downstream of a tangential blowing device. Hence, the boundary layer thickness cannot be robustly defined as a percentage of the freestream velocity, since the velocity profile is not monotonically increasing throughout the boundary layer. In order to avoid such problems, the boundary layer thickness was instead quantified using the displacement thickness δ^*, which is more robust to non-monotonic velocity profiles due to it being an integrated quantity, as can be seen from its definition

$$\delta^* = \int_0^\infty \left(1 - \frac{u(z)}{u_\infty}\right) \mathrm{d}z, \tag{3.2}$$

where the local velocity $u(z)$ is calculated as

$$u(z) = \sqrt{\frac{2q(z)}{\rho_s}}. \tag{3.3}$$

The dynamic pressure $q(z)$ is computed from the total pressure measurements using the compressible flow relation

$$q(z) = \frac{\gamma}{\gamma+1} P_s \left(\left(\frac{P_t(z) - P_s}{P_s} + 1 \right)^{\frac{\gamma-1}{\gamma}} - 1 \right), \tag{3.4}$$

where $\gamma = 1.4$ is the ratio of specific heats for air.

Influence on force measurements

The influence from the tangential blowing system on the forces measured on two vehicles, a notchback Volvo S60 and a squareback Volvo V60, was investigated for the seven different parameters shown in Table 3.1. The cars were chosen to be as similar as possible, with the exception of the different rear end geometries. The investigated parameters were the same for both cars, besides that the bootlid spoiler on the notchback was substituted by aero blades on the squareback. Some of the tested configurations can be seen in Figure 3.3. These specific factors were chosen since they were expected to influence the flow in the wake and/or under the car, which were the two regions expected to be mostly influenced by the tangential blowing. The reference configuration was chosen as the configuration with the expected highest drag: high ride height, open cooling, and no aerodynamic add-ons.

The investigation was performed using a 2^{7-3}_{IV} fractional factorial design of experiments approach, which allowed for quantification of both main effects and two-factor interactions [44]. However, since the design was of resolution IV, two-factor interactions were confounded with each other and could not be individually estimated. The confounding

Figure 3.1: *Prandtl tube mounted on custom built wing used for measurements of the longitudinal pressure distribution.*

Figure 3.2: *Boundary layer rake mounted on the traversing gear [2].*

(a) *Underfloor panels off*

(b) *Underfloor panels on*

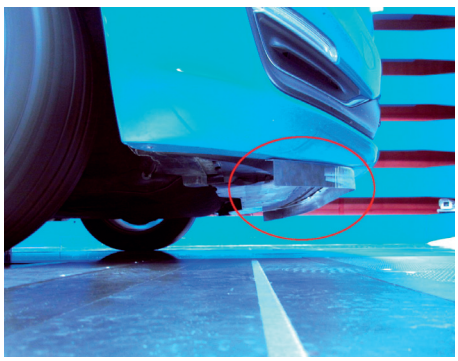

(c) *Air dam*

(d) *Front wheel deflector*

(e) *Aero blades (squareback only)*

(f) *Bootlid spoiler (notchback only)*

Figure 3.3: *Some of the configurations tested during the investigations on the influence of tangential blowing on the measured aerodynamic forces [2].*

Table 3.1: Factors investigated for the study on the influence of the tangential blowing system, their encodings and their levels in the experimental design. Ride height is given relative to the trim height at curb+2 weight.

Factor	Encoding	Low level	High level
Ride height	A	−15 mm	0
Bootlid spoiler/aero blades	B	Off	On
Air dam	C	Off	On
Underfloor panels	D	Off	On
Front wheel deflectors	E	Off	On
Covered rims	F	Off	On
Cooling flow	G	Closed	Open

Table 3.2: Confounding structure for the two factor interactions in the employed 2^{7-3}_{IV} fractional factorial design.

Interaction	Confounding structure
AB	AB + CE + FG
AC	AC + BE + DG
AD	AD + CG + EF
AE	AE + BC + DF
AF	AF + BG + DE
AG	AG + BF + CD
BD	BD + CF + EG

pattern for the design is shown in Table 3.2, where it can be seen that for example the interaction between ride height and bootlid spoiler/aero blades (AB) was confounded with the interactions between air dam and front wheel deflectors (CE), as well as covered rims and cooling flow. This meant that only the sum of these interactions could be estimated, but not their individual values. This limitation was the price paid for the limited number of test runs, 16, required by the chosen design. In order to allow for individual estimation of all two-factor interactions, a design of resolution V would be needed, which would require 64 runs. This fourfold increase in the number of runs was not feasible since it would not be possible to fit into the wind tunnel time allotted for this investigation.

The aerodynamic forces on the car were measured for each run both with tangential blowing on and off, after which each force coefficient was compared to its counterpart for the baseline configuration with the same blowing setting. This resulted in two delta values to the baseline for each configuration; one with tangential blowing on, and one with blowing off. When investigating the sensitivity of the different parameters to the blowing, the interesting response to look at is the delta-of-deltas, i.e. the difference between the two deltas. In this way, the response will be zero for a parameter if its influence on the aerodynamic force is the same regardless of the tangential blowing setting.

3.2 Numerical studies

The numerical investigations can be divided into two separate studies; parametric studies of the flow in the empty wind tunnel, and investigations into the force differences for a vehicle caused by tangential blowing.

All simulations were performed using STAR-CCM+. For the empty tunnel investigations, both steady-state and unsteady simulations were performed. The investigations of tangential blower effects on a car were only performed using unsteady simulations. The respective setups are described in more detail below.

3.2.1 Empty wind tunnel investigations

The empty wind tunnel simulations were performed for a full scale numerical model of the Volvo Cars aerodynamic wind tunnel. An overview of the tunnel geometry used in the computations can be seen in Figure 3.4. The geometry contains the settling chamber and contraction, followed by the slotted walls test section and diffuser, after which an extension was added to reduce the impact of the outlet condition on the flow in the test section. The geometry precision compared to the physical tunnel is believed to be good, with exceptions for excluded objects in the plenum outside of the slotted walls. However, it is not believed that the omission of these objects (cables, ladders, etc.) had a significant impact on the flow in the test section.

It was decided not to include the full circuit of the tunnel, based on the findings by Nayani et al. [32]. As previously described, they found that modeling the fan and the flow conditioning devices such as anti-turbulence screens greatly increased the complexity of the simulations without improving the prediction of the test section flow.

The inlet was set to a mass flow inlet, with the mass flow set in such a way that the velocity was 140 km/h at a point 1.2 m above the turntable centre. This corresponded to the position for which the wind speed was calibrated in the physical wind tunnel. The main outlet was set to a standard pressure outlet condition.

In order to simulate the boundary layer control system, all subsystems except for the basic suction scoop were modeled using patches on the flat floor, as drawn in Figure 2.3. A part of the basic suction scoop was included in the computational domain, with a prescribed mass flow as outlet condition. The included geometry corresponds to the part of the scoop sketched in the same figure. The moving belts were modeled with a moving wall boundary condition, while the distributed suction regions needed special attention. The approach used was that of Cyr et al. [36], where the distributed suction was modeled with a custom boundary condition that can be viewed as a slip-wall with a prescribed wall-normal velocity component to account for the mass flow removed from the test section by the system.

The mass removed by the basic and distributed suction was reinjected into the simulation domain using mass flow inlets at the same locations as in the physical tunnel. However,

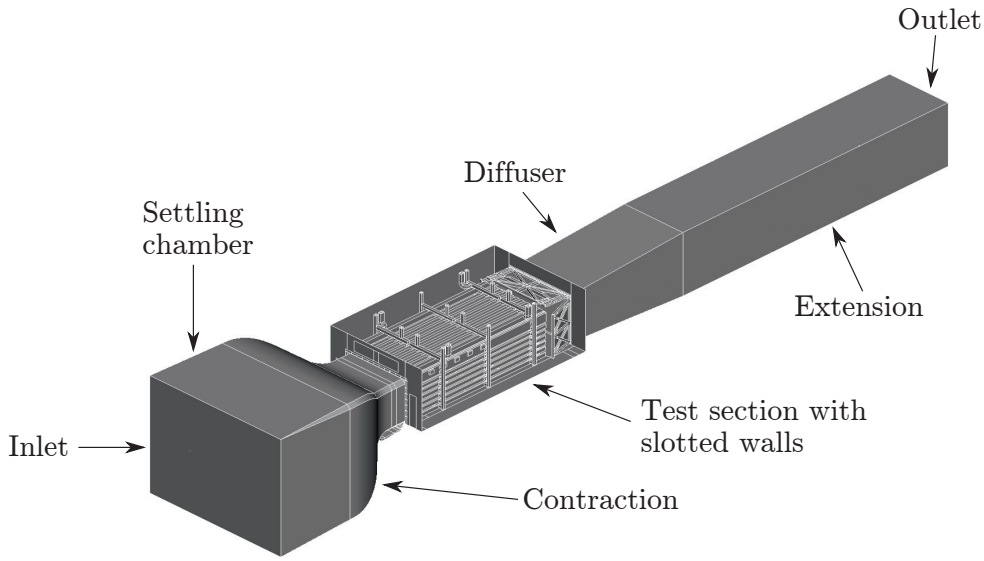

Figure 3.4: *Wind tunnel geometry used in the simulations [1].*

Table 3.3: Parameters investigated in the longitudinal pressure distribution study, their encodings and their levels in the experimental design.

Parameter	Encoding	Low level	Baseline	High level
Inlet yaw angle	A	$-1°$	$0°$	$1°$
Inlet pitch angle	B	$-1°$	$0°$	$1°$
Scoop mass flow	C	-20%	$-23.02\,\mathrm{kg/s}$	$+20\%$
1^{st} suction mass flow	D	-20%	$-5.18\,\mathrm{kg/s}$	$+20\%$
2^{nd} suction mass flow	E	-20%	$-1.38\,\mathrm{kg/s}$	$+20\%$
Belt speed	F	-20%	$38.89\,\mathrm{m/s}$	$+20\%$

no air was injected through the tangential blowers, which were omitted from the empty tunnel simulations due to uncertainties on how they should be simulated and the belief that their impact on the investigated flow quantities was small.

Steady-state parametric study

A design of experiments approach was employed in order to estimate the influence from six different boundary conditions in the numerical wind tunnel on the longitudinal pressure distribution on the centre line of the test section. The six parameters were inlet yaw and pitch angles, basic scoop suction mass flow, first and second distributed suction mass flows, and moving belt speed. The parameters and their respective levels can be seen in Table 3.3.

Design of experiments In order to allow for quadratic effects and two-factor interactions, a Box-Behnken design [44] was used, which required 61 runs. The Dakota framework [45] was used to construct the design matrix and to estimate the effects, defined as the polynomial coefficients c_i and c_{ij} in the fitted model

$$\hat{f}(\mathbf{x}) = c_0 + \sum_{i=1}^{6} c_i x_i + \sum_{i=1}^{6} \sum_{j \geq i}^{6} c_{ij} x_i x_j, \tag{3.5}$$

where $\mathbf{x}$ denotes the parameters, and c_0 corresponds to the mean response over all runs. In order to compare relative changes in each parameter, which was important due to the varying ranges of the parameters, the parameters were scaled to the range $[-1, 1]$ before fitting the data to equation (3.5). The judgement of statistical significance was done using the method for analysis of unreplicated factorials by Lenth [46]. The method is based on the definition of a Margin of Error (ME) and a Standard Margin of Error (SME), where an effect can be deemed as active if its absolute value is larger than the SME, and inactive if its value is smaller than the ME. The method is not conclusive for effects whose value falls in between the two margins of error.

Since the chosen Box-Behnken design is a three level ditto, the responses will divide into three separate groups if one of the factor effects is dominating the others in terms of magnitude. The spread within the groups will then be caused by the other, still significant, effects. If the responses are more uniformly spread out in the range of the output, it is likely that a number of effects are active and of similar magnitude.

Data sampling The response considered was the gradient of the longitudinal pressure distribution, which was sampled on the centre line of the test section, from $x = -3.8\,\mathrm{m}$ to $x = 7.5\,\mathrm{m}$, where $x = 0$ corresponds to the centre of the turntable. The line was divided into three parts; $-3.8\,\mathrm{m} \leq x \leq -0.5\,\mathrm{m}$, $-0.5\,\mathrm{m} \leq x \leq 3.5\,\mathrm{m}$ and $3.5\,\mathrm{m} \leq x \leq 7.5\,\mathrm{m}$, on which the mean of the gradient of the sampled pressure distribution was used to estimate the effects in equation (3.5). The seemingly random choice of the three zones was based on the behaviour of the pressure gradient, such that each zone represent a region with clear gradient differences.

Simulation settings The steady-state simulations of the empty wind tunnel utilized the $k - \varepsilon$ turbulence model. The mesh was of trimmed type and contained 186 million volumetric cells, with 10 prism layers and a near wall thickness of 2 mm. This resulted in y^+-values of between 50 and 130 on the test section walls.

Unsteady parametric study

Since the computational cost for an unsteady simulation is much greater than for a corresponding steady-state simulation, the number of investigated parameters were reduced from six to one. The parameter chosen was the basic scoop suction, as it had shown to

Table 3.4: Summary of the settings for both steady-state and unsteady simulations.

	Value	
Setting	Steady-state	Unsteady
Number of cells	$186 \cdot 10^6$	$100 \cdot 10^6$
y^+	$50 - 130$	
Spatial discretisation	2^{nd} order upwind	Hybrid-BCD
Turbulence model	Realizable $k - \varepsilon$	SST $k - \omega$ IDDES
Number of iterations	3000	N/A
Averaging time [s]	N/A	3
Time step [s]	N/A	$2.5 \cdot 10^{-4}$

be the most influential in the steady-state parametric study. In a further effort to reduce the computational cost, some work was spent on trying to reduce the mesh size without sacrificing fidelity in regions with large gradients. In order to achieve this, the number of prism layers was reduced from 10 to one on the wall surfaces facing away from the test section, such as the back sides of the wall slats and the reentry flaps. Furthermore, the base size for the mesh was increased slightly, leading to a maximum cell size of 12 mm in the wall slots, and 96 mm in the approximately inviscid core of the freestream in the test section. The redistribution of cells allowed for a reduction of the mesh size compared to the steady-state case, while still resolving the flow in the shear layer in the slots of the walls and keeping the near wall resolution. The final mesh consisted of 99 million trimmed volumetric cells, compared to the 186 million for the steady-state simulations.

The simulations were run using the Improved Delayed Detached Eddy Simulation (IDDES) formulation [47] of the SST $k-\omega$ turbulence model. The unsteady solution was initialized using a steady-state solution, after which it was run for 2.5 seconds to allow for initial transients to vanquish. The flow field was then averaged for 3 seconds with a timestep of $\Delta t = 2.5 \cdot 10^{-4}$ s to obtain the averaged longitudinal pressure distribution. In order not to introduce excessive numerical dissipation that might dampen the resolved turbulence, the Hybrid-BCD differencing scheme was used. This scheme is a blend between an upwind scheme and a bounded central differencing scheme, and is expected to provide a good trade-off between stability and accuracy. Table 3.4 provides an overview of the settings for both the steady-state and the unsteady setups.

3.2.2 Tangential blowing investigations

All simulations were performed using the IDDES formulation of the SST $k - \omega$ model. The full geometry of the wind tunnel was not included; instead, a simple rectangular box was used. The moving ground system was represented by the five moving belts and their corresponding tangential blowers, as shown in Figure 3.5. The upstream suction systems were omitted and their removal of an incoming boundary layer was achieved by using a symmetry boundary condition for the upstream section of the ground. As for the empty

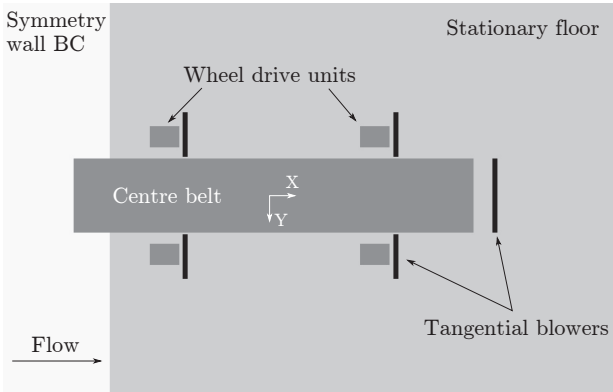

Figure 3.5: *Moving ground system as modeled during the tangential blowing investigations [2].*

tunnel simulations, the belts were modeled as walls with a prescribed tangential velocity.

Considering the geometry of the tangential blowers described in section 2.5.1, it is clear that a considerable amount of cells would be needed in order to resolve the flow at the blowing slots. In order to avoid the prohibitively large computational cost associated with such high resolution, the blowers were modeled using the approach introduced by Olander [41]. In this approach, each tangential blower is modeled as a patch on the floor, through which a mass flow is injected nearly parallel to the ground. This method deviates slightly from the method used by Wang et al. [48], who instead of injection of mass simulated the influence from the tangential blowing on the boundary layer by prescribing a high velocity on a patch of the floor representing the tangential blower. It is believed that the approach taken in the present work is more representative for the physical tunnel, since it accounts for the injected mass.

The mesh consisted of 77 million trimmed cells, using 12 prism layers with a near wall thickness of $0.0075 - 0.025\,\text{mm}$ on the upper body of the car to resolve the boundary layer to $y^+ < 1$. On the underbody and in the engine bay, one 1 mm thick prism layer was built. The stationary part of the ground was covered with 8 prism layers with a near wall thickness of 1 mm, accompanied with an anisotropic refinement of the cells close to the ground, in order to account for the boundary layer buildup. The mesh on the centre plane of the car can be seen in Figure 3.6.

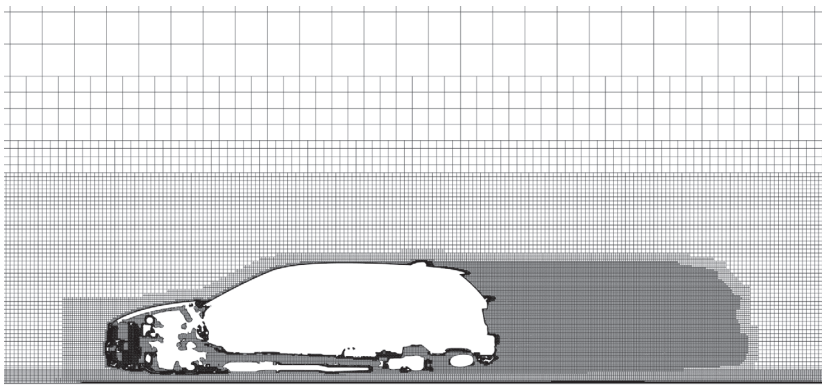

Figure 3.6: *Computational mesh at centre plane of the car.*

4 Results and discussion

This chapter contains the results of the investigations described in the previous chapters. It begins with the parametric studies of the longitudinal pressure gradient in the empty wind tunnel. These investigations has been divided into steady-state and unsteady studies. After this, the results for the tangential blowing investigations are presented, beginning with the empty tunnel boundary layer and followed by the influence from the blowing onto the measured forces.

4.1 Steady-state parametric study of the longitudinal pressure gradient

The pressure coefficient sampled on the wind tunnel centre line for all 61 runs in the parametric study can be seen in Figure 4.1a. It can be noted that the overall behaviour of the pressure distributions is not significantly changed between the runs. This indicates that the main reason for the longitudinal pressure distribution having a certain behaviour is not the inlet angularity or the boundary layer control systems, but rather the geometrical features of the nozzle, test section walls and collector, which corresponds well with the classical theory of wind tunnel design [5–7, 13].

Considering the gradients of the longitudinal pressure distributions $\mathrm{d}Cp/\mathrm{d}x$ in Figure 4.1b, it can be seen that there are some differences between the behaviours of the distributions. When examining the curves it can be seen that they are all approximately equal at $x = -0.5\,\mathrm{m}$ and $x = 3.5\,\mathrm{m}$, which justifies the division of the sampled region into three zones as described in section 3.2.1.

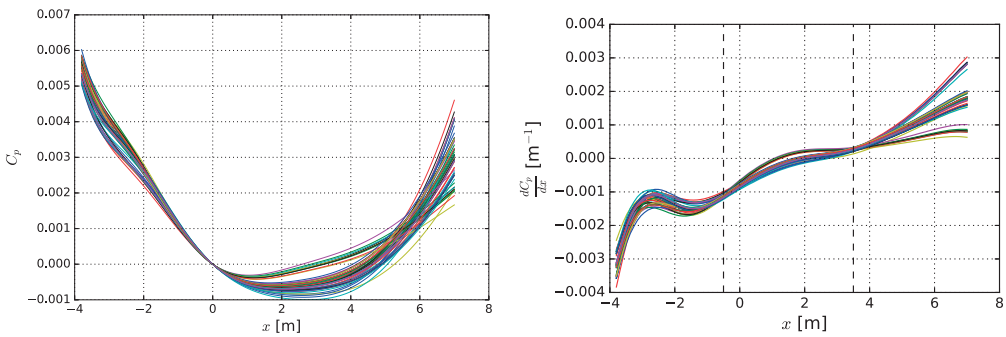

(a) *Longitudinal pressure distributions. All curves are shifted such that $C_p = 0$ at $x = 0$.*

(b) *Pressure gradients*

Figure 4.1: *Longitudinal pressure distributions and -gradients for all 61 runs in the parametric study [1].*

4.1.1 Pressure gradient in the upstream region

When looking at the upstream region $-3.8\,\mathrm{m} \leq x \leq -0.5\,\mathrm{m}$ in Figure 4.1b, the curves are somewhat scattered with no obvious grouping. The fact that no distinct groups are formed means that more than one of the tested factors are active, and of similar magnitude. This is confirmed by the effects shown in Figure 4.2a, where many of the effect bars extend beyond the Lenth SME lines. It can be seen that all the linear effects in the three suction parameters (C, D and E in Table 3.3) are active and of comparatively large magnitude, albeit with different signs between the basic suction (C) and the two distributed suctions (D and E). Furthermore, the basic suction shows a significant second-order effect (CC) and interactions with the distributed suctions (CD and CE), as well as interactions with the inlet yaw and pitch angles (AC and BC). However, it shall be noted that although statistically significant, all interactions except for CD are small in comparison to the dominating effects and thus not regarded as having an important influence on the pressure gradient in this region. The same can be said for the main effects for the two inlet angles.

It is expected that the suction systems have an impact in this region, since most of it is located above the distributed suction zones and of the three regions it is closest to the basic suction scoop.

4.1.2 Pressure gradient in the center region

Considering the center region $-0.5\,\mathrm{m} \leq x \leq 3.5\,\mathrm{m}$ in Figure 4.1b, it can be seen that the gradients have a relatively small magnitude in this region, which corresponds well with the flat pressure profiles in Figure 4.1a. For both figures, a group of curves are deviating slightly from the others, which is likely caused by a large effect. Normally a dominating effect would lead to three distinct groups instead of two, which indicates that a non-linear effect is active. This is confirmed when looking at the effects in Figure 4.2b, where it can be seen that the basic suction (C) is dominating, and that its second-order effect (CC) is active. The first distributed suction (D) is also active, which is likely also the case for the second distributed suction (E), due to its relative large effect. However, its magnitude is in between the Lenth ME and SME, which means that Lenth's method is not conclusive on its significance.

4.1.3 Pressure gradient in the downstream region

For the downstream region in Figure 4.1b, it can be seen that the curves divide into three very distinct groups. As mentioned in section 3.2.1, this corresponds to one dominating effect, which according to Figure 4.2c is the the basic suction (C). It can be seen that its magnitude is much larger than for the first distributed suction (D), which is the only other significant effect. The distributed suction is responsible for the spread within the three main groups, which under close inspection can be seen to each divide into three sub-groups, as is expected when there are two active effects with different magnitudes.

4.1.4 Final remarks

When considering the effects for all three regions in Figure 4.2, it is evident that of the tested parameters, the three suction mass flows are the most influential ones on the pressure gradient. This is expected as they alter the local flow velocities in the test section, as have been previously pointed out by Wickern et al. [30].

4.2 Unsteady parametric study of the longitudinal pressure gradient

The longitudinal pressure distribution sampled on the test section centre line for the three simulations in the unsteady parametric study can be seen in Figure 4.3. Results for both the corresponding cases in the steady-state parametric study and the distribution measured in the physical wind tunnel are included for comparison.

It can be seen that the unsteady simulations are able to predict the pressure distribution downstream of the turntable centre, $x > 0$, much better than their steady-state counterpart. The reason for this improvement is most probably due to that the unsteady simulations are able to account for the larger scales of the anisotropic turbulence in the shear layers in the side wall and roof slots. This claim is strengthened when considering the velocity fields in Figure 4.4, where it can be seen that the steady-state simulations predict thinner shear layers than the unsteady simulations.

Considering the region upstream of the turntable centre, $x < 0$, it can be seen that the change to the more realistic simulation model does not seem to have a significant impact on the pressure distribution. This can likely be attributed to the fact that the shear layers in the open area of the slotted walls and roof are still thin in this region, so that the shear layer thickness predicted by the two methods is similar. However, the present investigations give no clear insight into why the difference between both simulation techniques and the physical tunnel occurs in this region. This is an area that needs further investigations, but it is speculated that since the values for the mass flows through the distributed suction systems are unknown for the physical tunnel, the difference might be caused in part by erroneous mass flow values in the simulations. This is somewhat strengthened by the steady-state study, which indicated that the distributed suction has an impact on the pressure distribution in this part of the test section.

For the gradients of the longitudinal pressure, as shown in Figure 4.5, it can be seen that the behaviour is different for the unsteady simulations compared to the steady-state, which is expected since the underlying pressure distributions have changed significantly. When considering the region upstream of the turntable centre, the trends in the gradients when changing the scoop suction mass flow are similar for the two simulation approaches, which is expected due to their similar behaviour for the underlying pressure distribution. However, this changes in the downstream region, where for the unsteady simulations the curves are consistently ordered by their mass flow setting. For the steady-state simulations,

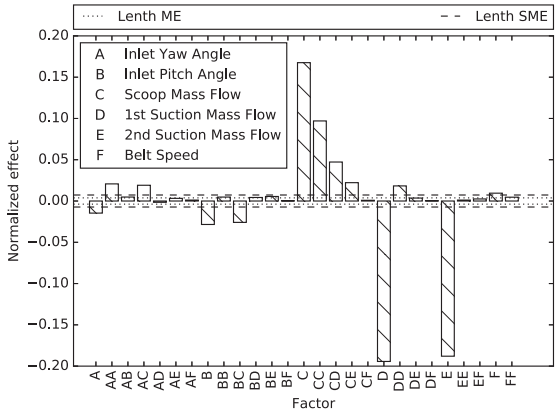

(a) *Front*

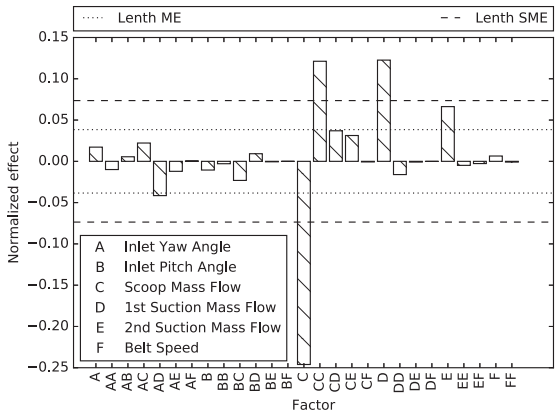

(b) *Center*

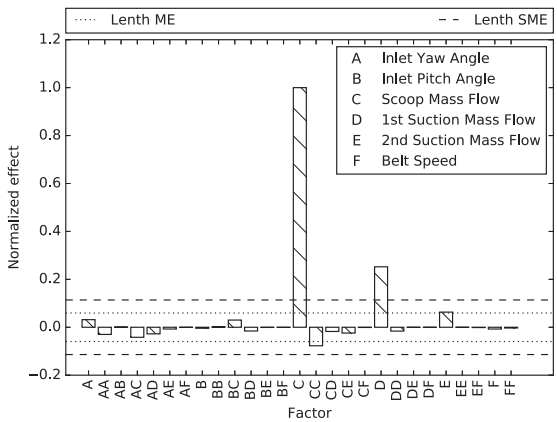

(c) *Rear*

Figure 4.2: *Effects on mean of the longitudinal pressure gradient for the three regions [1].*

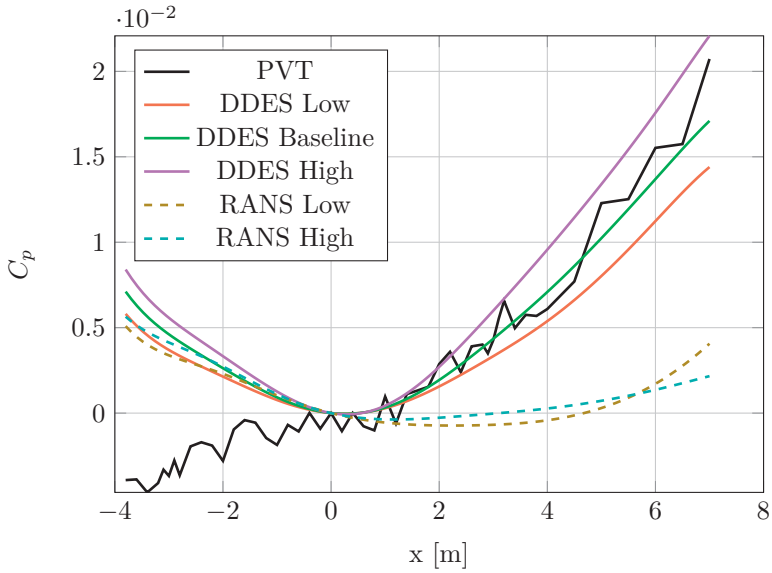

Figure 4.3: *Comparison between longitudinal pressure distributions for the physical wind tunnel (PVT) and both steady-state (RANS) and unsteady (DDES) simulations. High, low and baseline denote the scoop suction mass flow level as given in Table 3.3.*

the curves intersect at $x \approx 3.5\,\text{m}$. Downstream of this point, the behaviour with respect to the mass flow is opposite to the unsteady cases. The fact that the results from the unsteady simulations better matches the measurements from the physical tunnel, at least in this region, indicates that the gradient behaviour for the unsteady cases is the more correct of the two.

4.3 Tangential blowing investigations

Here, the results of the tangential blowing investigations are presented, starting with the boundary layer thickness in the empty tunnel. This is followed by the study on the influence on force measurements.

4.3.1 Boundary layer thickness

The displacement thickness behind each wheel drive unit tangential blower can be seen in Figure 4.6. The blowing slots span the region $520\,\text{mm} \leq |y| \leq 1120\,\text{mm}$, and the upstream positions of the WDU belts are indicated by the shaded regions. Comparing the displacement thickness between front and rear, it can be seen that the boundary layer is significantly thicker in the region outside of the influence of the blowers, $|y| \gtrsim 1150\,\text{mm}$.

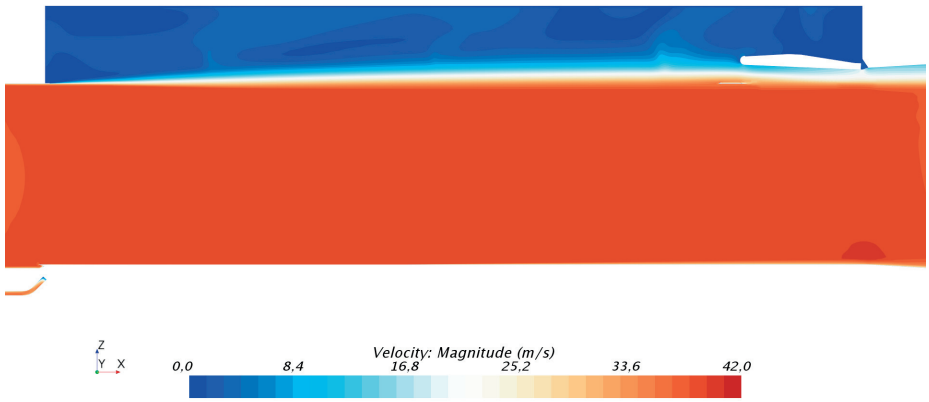

(a) *Steady-state*

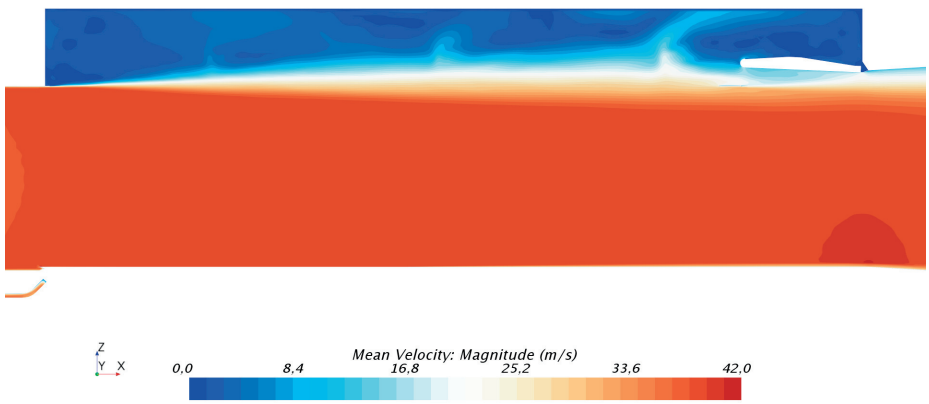

(b) *Unsteady*

Figure 4.4: *Velocity field on centre plane of the empty wind tunnel for steady-state and unsteady simulations, respectively. The unsteady flow field was averaged for 3 seconds.*

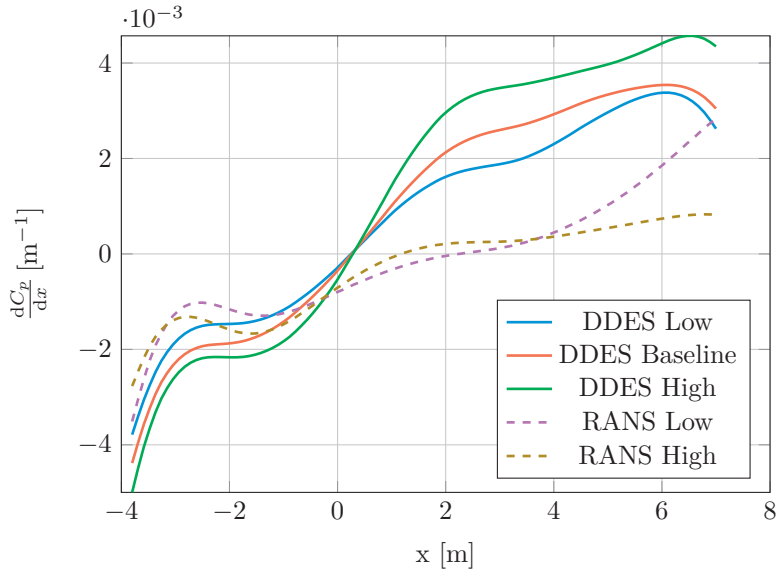

Figure 4.5: *Comparison between the gradient of the longitudinal pressure distributions for steady-state (RANS) and unsteady (DDES) simulations. High, low and baseline denote the scoop suction mass flow level as given in Table 3.3.*

This is expected since the boundary layer will grow on the stationary floor in between the front and rear wheel drive units.

Adding to the difference between front and rear, there is also an asymmetry between the left and right blowers, which is especially evident close to the centre belt for the front blowers in Figure 4.6a and 4.6b. It is hypothesised that the difference is more pronounced in this region due to a part of a nylon strip that was previously acting as a spacing between the centre belt and the surrounding stationary ground, but has fallen off piece by piece. The part believed to cause the sharp rise in displacement thickness close to the centre belt for the front left blower can be seen just upstream of the rake in Figure 3.2.

For the front blowers, a bump in the displacement thickness can be seen downstream of the edges of the wheel drive units. It is believed that this phenomenon is caused by a three-dimensional swirl originating from the interfaces between the stationary ground and the moving WDU belts. A similar effect would also explain the increase in boundary layer thickness seen close to the centre belt, i.e. for small $|y|$.

Considering the overall effect from the tangential blowing for all four blowers in Figure 4.6, it can be concluded that the tangential blowing system is effective at reducing the displacement thickness aft the wheel drive units. For the two lower velocities, the displacement thickness even becomes negative in some regions, mainly behind the WDU belts which helps in reducing the boundary layer thickness upstream of the blowers. This would mean that the blowing speed should ideally be reduced, but since the displacement

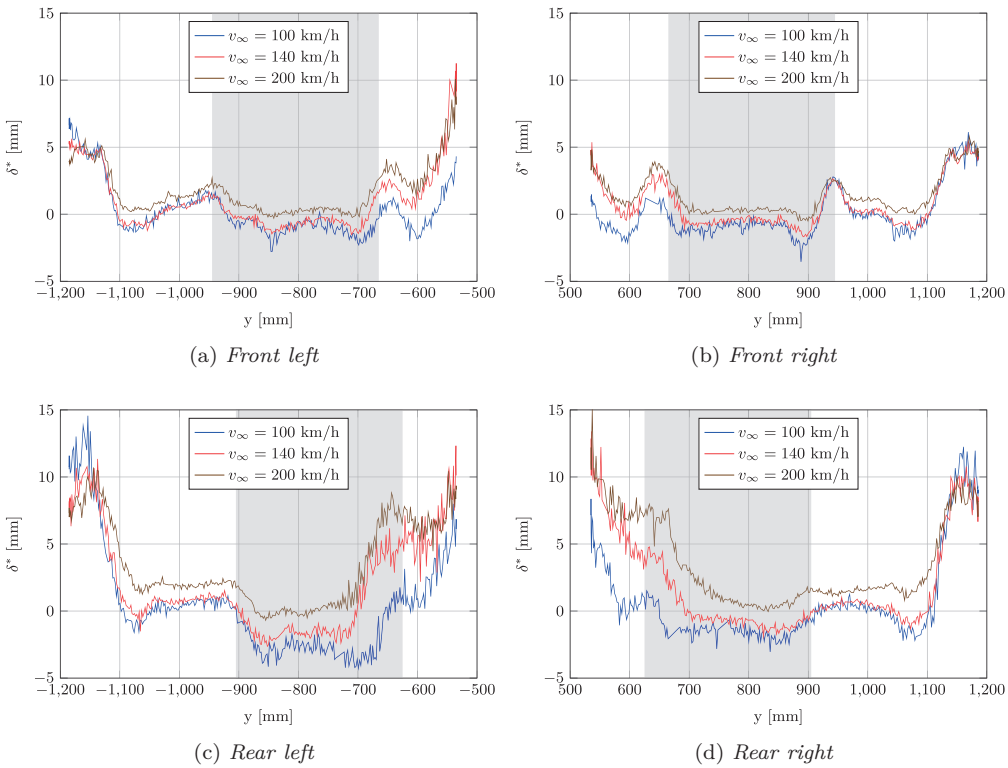

(a) *Front left* (b) *Front right*

(c) *Rear left* (d) *Rear right*

Figure 4.6: *Displacement thickness across the tangential blower slot* 800 mm *behind each wheel drive unit blower with all boundary layer systems active. Shaded areas represent the location of the upstream wheel drive units [2].*

thickness profile is non-uniform, this would lead to a less effective boundary layer reduction in other areas. It can also be noted that the 200 km/h case shows consistently higher values for the displacement thickness for all four investigated blowers. This is likely due to the fact that at such high freestream velocities, the tangential blowing system is very close to its maximum capacity.

Verification of CFD blower modeling

Figure 4.7 shows a comparison between physical measurements and CFD simulations for the front left blower without a car. It can be seen that the simulation is able to predict well the boundary layer outside of the region influenced by the tangential blowing $|y| \gtrsim 1150$ mm, and that the overall behaviour of the displacement thickness profile behind the blower is captured. A small effect from the WDU belt can also be seen as a slight drop in the profile. However, the bumps believed to be caused by the interface between

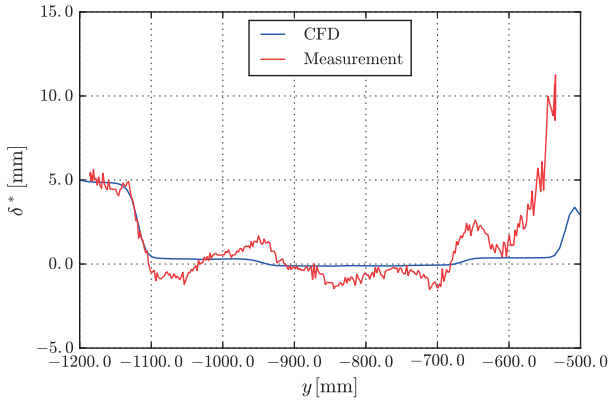

Figure 4.7: *Comparison of displacement thickness, δ^*, between measurement and simulation* 800 mm *downstream of the front left blower in the empty tunnel for the freestream velocity* 140 km/h *[2].*

the stationary ground and the moving belt are not seen in the simulation. This is also the case for the boundary layer thickening close to the centre belt. It is believed that both these discrepancies are caused by the fact that the floor in the CFD simulations is completely flat, which is not the case in the physical wind tunnel. Furthermore, it is likely that the mesh resolution is not fine enough to capture the buildup of a three-dimensional swirling motion caused by the two neighbouring floor patches of different velocities.

It shall be noted that even though the displacement thickness is well predicted, it is possible that the velocity profile in the wall-normal direction throughout the jet is not. It is plausible that such discrepancy between the simulations and the physical measurements would impact the results of the car simulations performed with tangential blowing, although it is believed that such influence will be of a local nature and that the displacement thickness is a good measure of the global impact from the blowing on the flow field.

4.3.2 Influence on force measurements

The main effects and two-factor interactions on the measured force coefficient deltas and delta-of-deltas for both the notchback and the squareback can be seen in Figure 4.8. The horizontal black lines in the delta-of-deltas plots show the wind tunnel repeatability, as shown in Table 2.5, which is used to judge whether an effect is of significant magnitude or not.

Drag Considering the effects for drag in Figures 4.8a and 4.8b, it can be seen that the squareback shows a considerably higher sensitivity to tangential blowing than the notchback, for which only the air dam (C) and cooling blanking (G) show significant,

however small, effects on the delta-of-deltas. These factors are also significant for the squareback, together with ride height (A) and front wheel deflectors (D). However, the magnitudes of the effects are much larger for the squareback, which is especially clear for the cooling blanking, for which $\Delta\Delta C_D = 0.008$, or 47% of the cooling drag measured with the blowing turned off. It is believed that the differences between the two vehicles is caused by the larger base area of the squareback, since the only major geometrical difference compared to the notchback is the shape of the rear end.

It can be noted that even though the effects for the delta-of-deltas change sign, the sign of ΔC_D compared to the baseline is not changed by the tangential blowing, except for the air dam (C) for both the notchback and the squareback. For this device, the small decrease in drag seen without tangential blowing vanishes when the blowing is turned on.

Lift In contrast to the results for drag, the two vehicles show a similar sensitivity to tangential blowing for the front lift, as can be seen in Figures 4.8c and 4.8d. Both cars show a measurable sensitivity for the air dam (C) and the rim covers (F), as well as one interaction each; AD for the notchback and AB for the squareback. It can also be noted that the AD interaction show a clear influence on ΔC_{LF} for both vehicles. Consulting the confounding pattern in Table 3.2 gives that this interaction also includes the interaction between the air dam and the cooling blanking (CG), both of which show a large influence on ΔC_{LF}.

Even though the effects on $\Delta\Delta C_{LF}$ are clearly larger than the repeatability of the wind tunnel, the differences between tangential blowing on and off are relatively small in comparison to the measured values for ΔC_{LF}.

Looking at the rear lift in Figures 4.8e and 4.8f, it can be seen that none of the effects for the delta-of-deltas are deemed significant by the employed criterion. This is partly due to the higher repeatability figures for rear lift given in Table 2.5.

Numerical results

As previously discussed, the configuration most sensitive to tangential blowing is the cooling blanking for the squareback. However, the force measurements in the wind tunnel give no guidance on where on the vehicle the differences occur, and how the flow field is affected by the tangential blowing. To investigate where the differences occur, the pairwise differences between four simulations are analysed. The four cases are all for the squareback, with open and closed cooling, and with and without tangential blowing.

In order to more clearly identify local differences between forces or in the flow field, a change of view is necessary compared to the physical tests. For the wind tunnel results, two drag deltas were defined, one for each blower mode. Using the closed cooling as an example gives

$$\Delta C_{D_{\text{closed, TB on}}} = C_{D_{\text{closed, TB on}}} - C_{D_{\text{baseline, TB on}}}$$
$$\Delta C_{D_{\text{closed, TB off}}} = C_{D_{\text{closed, TB off}}} - C_{D_{\text{baseline, TB off}}}.$$

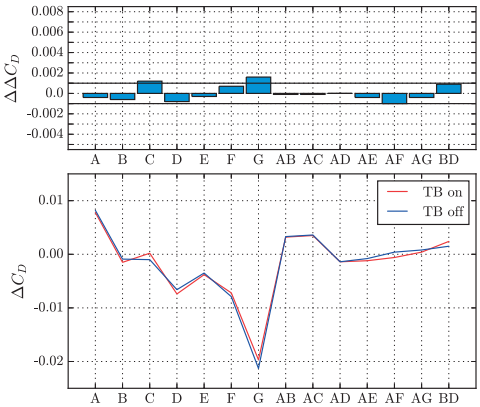

(a) *Effects on drag, notchback*

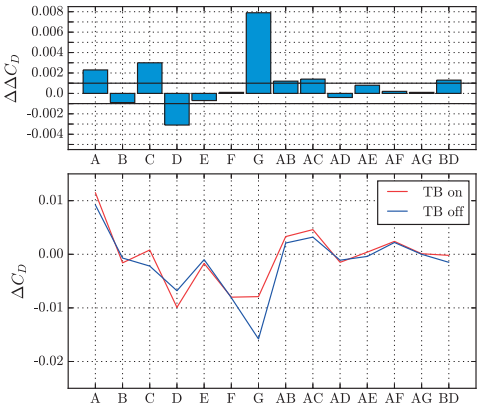

(b) *Effects on drag, squareback*

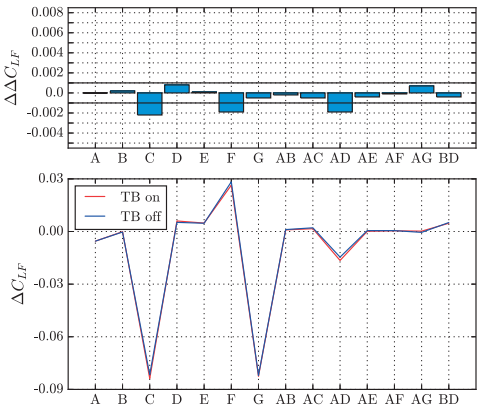

(c) *Effects on front lift, notchback*

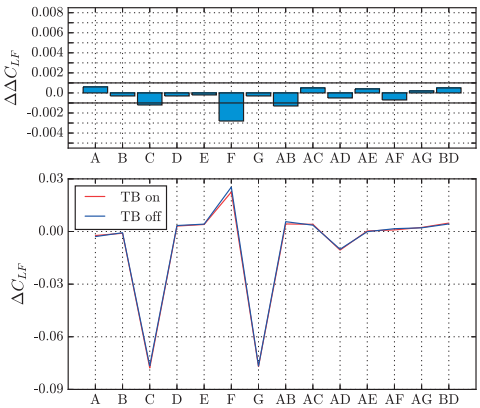

(d) *Effects on front lift, squareback*

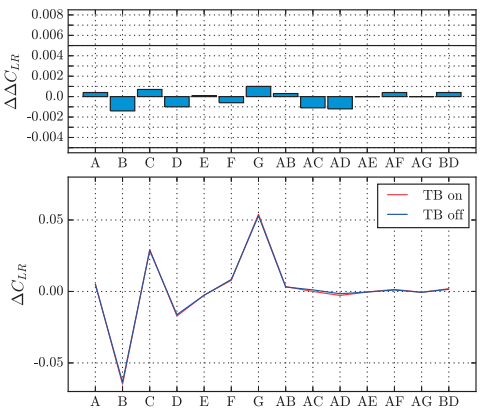

(e) *Effects on rear lift, notchback*

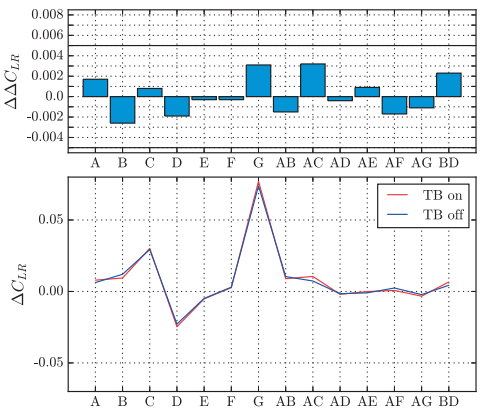

(f) *Effects on rear lift, squareback*

Figure 4.8: *Effects from tangential blowing on force deltas and delta-of-deltas. The horizontal black lines in the bar plots indicate the repeatability of the wind tunnel [2].*

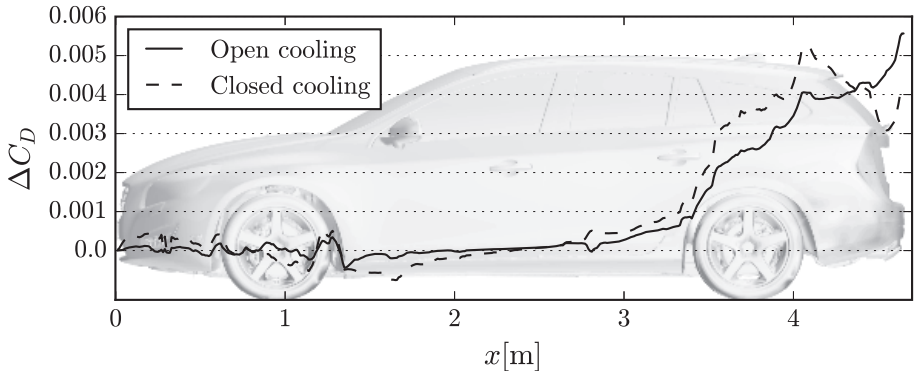

Figure 4.9: *Accumulated drag difference from CFD between tangential blowing on and off over the length of the car [2].*

For the numerical simulations, one drag delta is instead used as

$$\Delta C_{D_{\text{closed}}} = C_{D_{\text{closed, TB on}}} - C_{D_{\text{closed, TB off}}}.$$

This is done in order to have results more similar in magnitude, thus facilitating identification of small differences.

In order to identify regions on the car that contribute to the drag difference observed in the wind tunnel, consider the accumulated drag difference along the length of the vehicle in Figure 4.9. Noting the difference between the curves at the downstream end of the car, it can be seen that the trend for $\Delta\Delta C_D$ seen in the wind tunnel is captured in the simulations. However, for the physical measurements $\Delta\Delta C_D = 0.008$, while $\Delta\Delta C_D \approx 0.002$ for the numerical model. This disagreement in magnitude between CFD and the wind tunnel is suspected to be caused by either the fact that the numerical car model is not the exact same variant as the test object, or by insufficiencies in the numerical approach. However, no extensive investigations have been performed in order to root out the cause of these discrepancies.

Furthermore, Figure 4.9 shows that the major differences occur in the rear of the car, around the rear wheels and on the base. Considering the base, it can be seen that the trends shifts; while the tangential blowing decreases the drag contribution for the closed cooling, it slightly increases the contribution for the open cooling case. This effect is also noticeable when looking at the base pressure differences in Figure 4.10. For the open cooling, the tangential blowing slightly reduces the pressure on the right hand side of the rear hatch, while it slightly increases the pressure on the left hand side. These effects almost cancel out, which results in an almost flat curve in this region in Figure 4.9. Looking at the closed cooling case, it can be seen that the pressure is increased on most parts of the hatch, thus reducing the drag influence as seen in the accumulated drag.

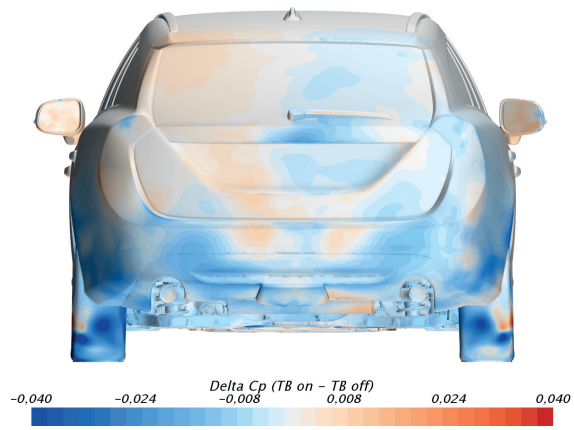

(a) *Open cooling*

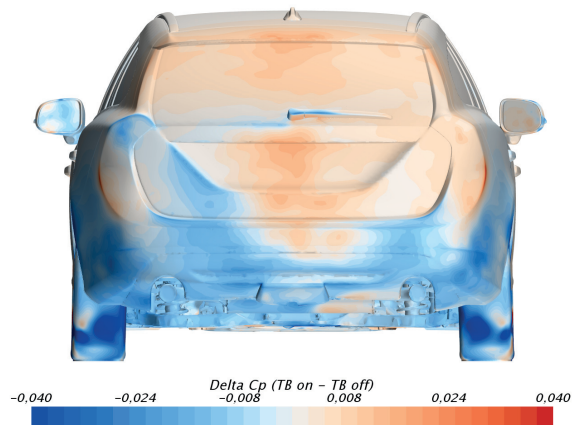

(b) *Closed cooling*

Figure 4.10: *Difference in pressure coefficient, ΔC_P, on the base of the squareback [2].*

5 Summary and conclusions

The purpose of this work has been twofold. First, the influence of a set of boundary conditions on the longitudinal pressure distribution in simulations of a slotted wall automotive wind tunnel was investigated. This was followed by and examination of the impact from tangential blowing in the moving ground system, both on the floor boundary layer in the empty tunnel and on the aerodynamic forces measured on vehicles.

First, a parametric study was performed for six boundary conditions for simulations of a detailed numerical representation of the wind tunnel using steady-state CFD simulations. The boundary conditions studied were the inlet yaw and pitch angles, the speed of the moving belt, and the mass flows for the basic suction scoop and the two distributed suction zones. The study showed that even though the overall trend of the longitudinal pressure distribution was not changed by the parameters in their considered intervals, some effects could be seen. It was shown that the three suction mass flows had statistically significant effects on the gradient of the longitudinal pressure distribution, and that the scoop mass flow was dominating, which was especially clear in the downstream region of the test section.

Following this, a reduced version of above parametric study was performed for only the basic scoop suction, using unsteady CFD simulations. It was observed that the unsteady method was able to predict the pressure distribution in the downstream region of the turntable much better than its steady-state counterpart when compared to measurements from the physical tunnel. This improvement was attributed to a better representation of the shear layer in the slots of the slotted side walls and roof. However, no improvement was seen for the behaviour in the region upstream of the turntable centre, which was poorly predicted in both methods. It was hypothesised that this was, at least partly, caused by possibly incorrect values for the mass flows through the distributed suction systems in the simulations, as the actual values in the physical tunnel are unknown.

Finally, the tangential blowing subsystem of the moving ground system was investigated using both experiments and numerical simulations. Measurements of the displacement thickness profile downstream of the tangential blowers showed that the blowing does reduce the momentum loss in the boundary layer as expected, but that some non-uniformities occur in the vicinity of interfaces between moving belts and stationary floor. Furthermore, it was shown that CFD simulations were able to predict the overall behaviour of the measured profiles, even though the non-uniformities mentioned were not captured.

The investigation of the impact from the tangential blowing on the measured vehicle forces was conducted using a design of experiments approach involving two vehicles in seven configurations each. It was found that of the two cars, the squareback with its larger base area was more sensitive to tangential blowing. Furthermore, configurations altering the underbody flow were more sensitive to the blowing than those only affecting the flow in the base wake. Using CFD simulations of the most sensitive case, the squareback with open and closed cooling, to identify the differences between tangential blowing on and off showed that the main influence on the drag was acting in the rear of the vehicle, mainly

in the region of the rear wheels and the base.

5.1 Future work

As mentioned in the introduction, the present work is part of a larger project aimed at increasing the understanding of slotted wall wind tunnels in automotive aerodynamics. This thesis has of course not exhausted the topic, but leaves plenty of challenges for further research.

It was shown that the use of unsteady CFD greatly improved the simulation accuracy when it comes to predicting the longitudinal pressure distribution in the test section of the wind tunnel, but that inaccuracies still occur in some regions. According to the given hypothesis for the cause of these imprecisions, it is hopefully possible to improve the predictions by optimizing the suction mass flow values used in the simulations. Since the actual mass flows for a given freestream wind speed are unknown for the physical tunnel, a feasible approach for such optimization could be to "reverse engineer" the problem by minimizing the differences between the simulated and measured pressure distributions under variation of the considered mass flows.

For the tangential blowing it was shown that turning the system on or off might have an impact on the force measurements. However, the present study does not provide any insights to whether one of the operating conditions is to prefer in terms of providing more similar results to the open road case that the wind tunnel is supposed to simulate. Unfortunately, such insights are hard to gain using experimental techniques due to the many difficulties associated with on-road testing. On the other hand, the flexibility of CFD simulations allows for free variation of the boundary conditions, making it an excellent tool for further research on the topic.

Furthermore, more measurements of the flow in the empty tunnel will be carried out in order to provide data for validation of the simulations. For example, measurements of flow angularity and dynamic pressure uniformity in locations not covered in the commissioning of the tunnel, such as at the nozzle outlet plane, could provide insights on whether discrepancies between simulation and physical tunnel originates in the simulation of the test section or are caused by upstream artifacts.

References

[1] E. Ljungskog, S. Sebben, A. Broniewicz, and C. Landström. A Parametric Study on the Influence from Boundary Conditions on the Longitudinal Pressure Gradient in CFD simulations of an Automotive Wind Tunnel. *Journal of Mechanical Science and Technology* **Accepted for publication** (2017).

[2] E. Ljungskog, S. Sebben, A. Broniewicz, and C. Landström. On the Effects of Wind Tunnel Floor Tangential Blowing on the Aerodynamic Forces of Passenger Vehicles. *SAE International Journal of Passenger Cars - Mechanical Systems* **10(2)**.2017 (2017). DOI: 10.4271/2017-01-1518.

[3] J. G. Olivier, J. A. Peters, and G. Janssens-Maenhout. *Trends in global CO2 emissions; 2016 Report*. The Hague: PBL Netherlands Environmental Assessment Agency; Ispra: European Commission, Joint Research Centre., 2016.

[4] *Global Technical Regulation No. 15 (Worldwide harmonized Light vehicles Test Procedure), Amendment 1, Appendix 1.* United Nations Global Technical Regulation ECE/TRANS/180/Add.15/Amend.1/Appendix 1. Mar. 8, 2017.

[5] K. Cooper. Bluff-body blockage corrections in closed-and open-test-section wind tunnels. *Wind Tunnel Wall Correction (AGARD-AG-336), BFR Ewald, ed., Advisory Group for Aerospace Research and Development, North Atlantic Treaty Organization, Neuilly-sur-Seine Cedex, France* (1998).

[6] J. B. Barlow, A. Pope, and W. H. Rae. *Low-speed wind tunnel testing*. 3. ed. New York: Wiley, 1999. 713 pp. ISBN: 978-0-471-55774-6.

[7] R. C. Pankhurst and D. W. Holder. *Wind-tunnel technique: an account of experimental methods in low-and high-speed wind tunnels*. Pitman, 1952.

[8] P. M. Waudby-Smith and W. J. Rainbird. "Some Principles of Automotive Aerodynamic Testing in Wind Tunnels with Examples from Slotted Wall Test Section Facilities". *SAE Technical Paper 850284*. Feb. 1, 1985. DOI: 10.4271/850284.

[9] H. C. Garner, E. W. Rogers, W. E. Acum, and E. C. Maskell. *SUBSONIC WIND TUNNEL WALL CORRECTIONS*. Oct. 1966.

[10] R. G. J. Flay, G. M. Elfstrom, and P. J. F. Clark. "Slotted-Wall Test Section for Automotive Aerodynamic Tests at Yaw". *SAE Technical Paper 830302*. Feb. 1, 1983. DOI: 10.4271/830302.

[11] S. RAIMONDO and P. CLARK. "Slotted wall test section for automotive aerodynamic test facilities". *12th Aerodynamic Testing Conference*. American Institute of Aeronautics and Astronautics, 1982. DOI: 10.2514/6.1982-585.

[12] M. Eng and T. Walker. "Investigation of Aerodynamic correction methods applied to a slotted wall wind tunnel". *Euromech Colloquium*. Vol. 509. 2009.

[13] E. Mercker and J. Wiedemann. "On the Correction of Interference Effects in Open Jet Wind Tunnels". *SAE Technical Paper 960671*. Feb. 1, 1996. DOI: 10.4271/960671.

[14] G. Wickern. "A Theoretical Approach towards the Self-Correcting Open Jet Wind Tunnel". *SAE Technical Paper 2014-01-0579*. Apr. 1, 2014. DOI: 10.4271/2014-01-0579.

[15] J. Wiedemann. "Some Basic Investigations into the Principles of Ground Simulation Techniques in Automotive Wind Tunnels". Feb. 1, 1989. DOI: 10.4271/890369.

[16] J. Wiedemann. "The Influence of Ground Simulation and Wheel Rotation on Aerodynamic Drag Optimization - Potential for Reducing Fuel Consumption". Feb. 1, 1996. DOI: 10.4271/960672.

[17] L. Larsson, L. Hammar, L. U. Nilsson, A. Berndtsson, K. Knutson, and H. Danielson. "A Study of Ground Simulation-Correlation between Wind-Tunnel and Water-Basin Tests of a Full-Scale Car". Feb. 1, 1989. DOI: 10.4271/890368.

[18] W.-H. Hucho, ed. *Aerodynamics of road vehicles: from fluid mechanics to vehicle engineering*. 4. ed. Warrendale, Pa: Society of Automotive Engineers, 1998. 918 pp. ISBN: 978-0-7680-0029-0.

[19] A. Klemin. A Belt Method of Representing the Ground. *Journal of the Aeronautical Sciences* **1**.4 (1934), 198–199. DOI: 10.2514/8.51.

[20] A. Cogotti. "Ground Effect Simulation for Full-Scale Cars in the Pininfarina Wind Tunnel". *SAE Technical Paper 950996*. Feb. 1, 1995. DOI: 10.4271/950996.

[21] G. Wickern and N. Lindener. "The Audi Aeroacoustic Wind Tunnel: Final Design and First Operational Experience". *SAE Technical Paper 2000-01-0868*. Mar. 6, 2000. DOI: 10.4271/2000-01-0868.

[22] P. Waudby-Smith, T. Bender, and R. Vigneron. "The GIE S2A Full-Scale Aeroacoustic Wind Tunnel". *SAE Technical Paper 2004-01-0808*. Mar. 8, 2004. DOI: 10.4271/2004-01-0808.

[23] J. Sternéus, T. Walker, and T. Bender. "Upgrade of the Volvo Cars Aerodynamic Wind Tunnel". *SAE Technical Paper 2007-01-1043*. Apr. 16, 2007. DOI: 10.4271/2007-01-1043.

[24] A. Cogotti. "The New Moving Ground System of the Pininfarina Wind Tunnel". *SAE Technical Paper 2007-01-1044*. Apr. 16, 2007. DOI: 10.4271/2007-01-1044.

[25] E. G. Duell, A. Kharazi, S. Muller, W. Ebeling, and E. Mercker. "The BMW AVZ Wind Tunnel Center". *SAE Technical Paper 2010-01-0118*. Apr. 12, 2010. DOI: 10.4271/2010-01-0118.

[26] H. Stumpf, P. Röser, T. Wiegand, B. Pfäfflin, J. Ocker, R. Müller, W. Eckert, and H.-U. Kroß. "The new aerodynamic and aeroacoustic wind tunnel of the Porsche AG". *15. Internationales Stuttgarter Symposium*. DOI: 10.1007/978-3-658-08844-6_54. Springer Vieweg, Wiesbaden, 2015, pp. 811–826.

[27] F. Wittmeier, A. Michelbach, J. Wiedemann, and V. Senft. "The New Interchangeable Three-belt System in the IVK Full-Scale Wind Tunnel of University of Stuttgart: Design and First Results". *SAE Technical Paper 2016-01-1581*. Apr. 5, 2016. DOI: 10.4271/2016-01-1581.

[28] A. Hennig, N. Widdecke, T. Kuthada, and J. Wiedemann. Numerical Comparison of Rolling Road Systems. *SAE International Journal of Engines* **4**.2 (June 9, 2011), 2659–2670. ISSN: 1946-3944. DOI: 10.4271/2011-37-0017.

[29] E. Mercker and J. Wiedemann. "Comparison of Different Ground Simulation Techniques for Use in Automotive Wind Tunnels". *SAE Technical Paper 900321*. Feb. 1, 1990. DOI: 10.4271/900321.

[30] G. Wickern, S. Dietz, and L. Luehrmann. "Gradient Effects on Drag Due to Boundary-Layer Suction in Automotive Wind Tunnels". *SAE Technical Paper 2003-01-0655*. Mar. 3, 2003. DOI: 10.4271/2003-01-0655.

[31] E. Mercker and H. Knape. “Ground Simulation with Moving Belt and Tangential Blowing for Full-scale Automotive Testing in a wind Tunnel”. Feb. 1, 1989. DOI: 10.4271/890367.

[32] S. Nayani, W. L. Sellers, A. F. Tinetti, S. E. Brynildsen, and E. L. Walker. “Numerical Simulation of a Complete Low-Speed Wind Tunnel Circuit”. *54th AIAA Aerospace Sciences Meeting*. American Institute of Aeronautics and Astronautics, Jan. 4, 2016.

[33] O. Fischer, T. Kuthada, N. Widdecke, and J. Wiedemann. “CFD Investigations of Wind Tunnel Interference Effects”. *SAE Technical Paper 2007-01-1045*. Apr. 16, 2007. DOI: 10.4271/2007-01-1045.

[34] O. Fischer, T. Kuthada, J. Wiedemann, P. Dethioux, R. Mann, and B. Duncan. “CFD Validation Study for a Sedan Scale Model in an Open Jet Wind Tunnel”. *SAE Technical Paper 2008-01-0325*. Apr. 14, 2008. DOI: 10.4271/2008-01-0325.

[35] O. Fischer, T. Kuthada, E. Mercker, J. Wiedemann, and B. Duncan. “CFD Approach to Evaluate Wind-Tunnel and Model Setup Effects on Aerodynamic Drag and Lift for Detailed Vehicles”. *SAE Technical Paper 2010-01-0760*. Apr. 12, 2010. DOI: 10.4271/2010-01-0760.

[36] S. Cyr, K.-D. Ih, and S.-H. Park. “Accurate Reproduction of Wind-Tunnel Results with CFD”. *SAE Technical Paper 2011-01-0158*. Apr. 12, 2011. DOI: 10.4271/2011-01-0158.

[37] C. Collin, S. Mack, T. Indinger, and J. Mueller. A Numerical and Experimental Evaluation of Open Jet Wind Tunnel Interferences using the DrivAer Reference Model. *SAE International Journal of Passenger Cars - Mechanical Systems* **9**.2 (Apr. 5, 2016). ISSN: 1946-4002. DOI: 10.4271/2016-01-1597.

[38] K. Horrigan, B. Duncan, P. Sivakumar, A. Gupta, and A. Wong. “Aerodynamic Simulations of a Class 8 Heavy Truck: Comparison to Wind Tunnel Results and Investigation of Blockage Influences”. *SAE Technical Paper 2007-01-4295*. Oct. 30, 2007. DOI: 10.4271/2007-01-4295.

[39] M. Heinecke, J. Beedy, K. Horrigan, and R. Sengupta. “Aerodynamic Study of a Production Tractor Trailer Combination using Simulation and Wind Tunnel Methods”. *SAE Technical Paper 2010-01-2040*. Oct. 5, 2010. DOI: 10.4271/2010-01-2040.

[40] S. Perzon. “On Blockage Effects in Wind Tunnels – A CFD Study”. *SAE Technical Paper 2001-01-0705*. Mar. 5, 2001. DOI: 10.4271/2001-01-0705.

[41] M. Olander. “CFD Simulation of the Volvo Cars Slotted Walls Wind Tunnel”. Masters Thesis. Chalmers University of Technology, 2011.

[42] A. Wall. “Simulating the Volvo Cars Aerodynamic Wind Tunnel with CFD”. Masters Thesis. Chalmers University of Technology, 2013.

[43] T. Bender. *Commissioning Report: PVT Ground Simulation Upgrade*. Internal Report 4147R269. Aiolos Engineering Corporation, Dec. 21, 2006.

[44] G. E. P. Box, J. S. Hunter, and W. G. Hunter. *Statistics for Experimenters: Design, Innovation and Discovery*. 2. ed. Wiley series in probability and statistics. Hoboken, N.J: Wiley-Interscience, 2005. 633 pp. ISBN: 978-0-471-71813-0.

[45] B. M. Adams et al. Dakota, A Multilevel Parallel Object-Oriented Framework for Design Optimization, Parameter Estimation, Uncertainty Quantification, and

Sensitivity Analysis: Version 6.0 User's Manual. *Sandia Technical Report SAND2014-4633* (July 6, 2014).

[46] R. V. Lenth. Quick and Easy Analysis of Unreplicated Factorials. *Technometrics* **31**.4 (1989), 469–473. ISSN: 0040-1706. DOI: 10.2307/1269997.

[47] M. L. Shur, P. R. Spalart, M. K. Strelets, and A. K. Travin. A hybrid RANS-LES approach with delayed-DES and wall-modelled LES capabilities. *International Journal of Heat and Fluid Flow* **29**.6 (Dec. 2008), 1638–1649. ISSN: 0142-727X. DOI: 10.1016/j.ijheatfluidflow.2008.07.001.

[48] F. Wang, Z. Yin, S. Yan, J. Zhan, H. Friz, B. Li, and W. Xie. Validation of Aerodynamic Simulation and Wind Tunnel Test of the New Buick Excelle GT. *SAE International Journal of Passenger Cars - Mechanical Systems* **10**.1 (Mar. 28, 2017), 195–202. ISSN: 1946-4002. DOI: 10.4271/2017-01-1512.